UPPSALA
UNIVERSITET

Digital Comprehensive Summaries of Uppsala Dissertations from the Faculty of Science and Technology 944

Experimental Studies of Charge Transport in Single Crystal Diamond Devices

SAMAN MAJDI

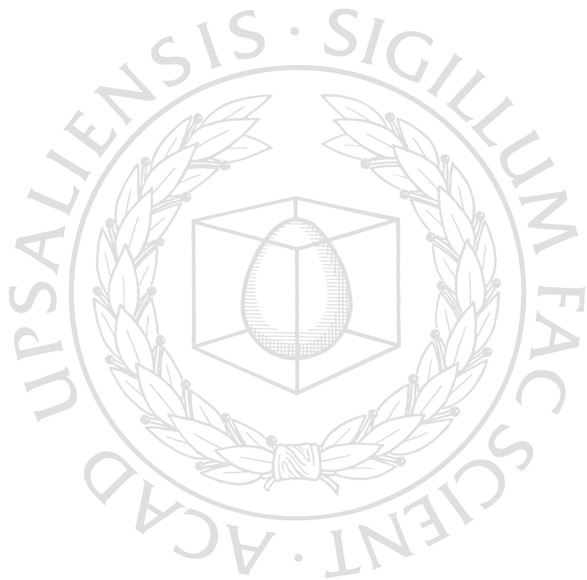

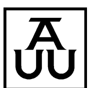

ACTA
UNIVERSITATIS
UPSALIENSIS
UPPSALA
2012

ISSN 1651-6214
ISBN 978-91-554-8391-3
urn:nbn:se:uu:diva-173599

Dissertation presented at Uppsala University to be publicly examined in Häggsalen, Lägerhyddsvägen 1, Ångströmlaboratoriet, Uppsala, Tuesday, June 5, 2012 at 13:15 for the degree of Doctor of Philosophy. The examination will be conducted in English.

Abstract

Majdi, S. 2012. Experimental Studies of Charge Transport in Single Crystal Diamond Devices. Acta Universitatis Upsaliensis. *Digital Comprehensive Summaries of Uppsala Dissertations from the Faculty of Science and Technology* 944. 67 pp. Uppsala. ISBN 978-91-554-8391-3.

Diamond is a promising material for high-power, high-frequency and high- temperature electronics applications, where its outstanding physical properties can be fully exploited. It exhibits an extremely high bandgap, very high carrier mobilities, high breakdown field strength, and the highest thermal conductivity of any wide bandgap material. It is therefore an outstanding candidate for the fastest switching, the highest power density, and the most efficient electronic devices obtainable, with applications in the RF power, automotive and aerospace industries. Lightweight diamond devices, capable of high temperature operation in harsh environments, could also be used in radiation detectors and particle physics applications where no other semiconductor devices would survive.

The high defect and impurity concentration in natural diamond or high-pressure-high-temperature (HPHT) diamond substrates has made it difficult to obtain reliable results when studying the electronic properties of diamond. However, progress in the growth of high purity Single Crystal Chemical Vapor Deposited (SC-CVD) diamond has opened the perspective of applications under such extreme conditions based on this type of synthetic diamond.

Despite the improvements, there are still many open questions. This work will focus on the electrical characterization of SC-CVD diamond by different measurement techniques such as internal photo-emission, *I-V*, *C-V*, Hall measurements and in particular, Time-of-Flight (ToF) carrier drift velocity measurements. With these mentioned techniques, some important properties of diamond such as drift mobilities, lateral carrier transit velocities, compensation ratio and Schottky barrier heights have been investigated. Low compensation ratios (N_D/N_A) < 10^{-4} have been achieved in boron-doped diamond and a drift mobility of about 860 cm^2/Vs for the hole transit near the surface in a lateral ToF configuration could be measured. The carrier drift velocity was studied for electrons and holes at the temperature interval of 80-460 K. The study is performed in the low-injection regime and includes low-field drift mobilities. The hole mobility was further investigated at low temperatures (10-80 K) and as expected a very high mobility was observed.

In the case of electrons, a negative differential mobility was seen in the temperature interval of 100-150K. An explanation for this phenomenon is given by the intervally scattering and the relation between hot and cold conduction band valleys. This was observed in direct bandgap semiconductors with non-equivalent valleys such as GaAs but has not been seen in diamond before.

Furthermore, first steps have been taken to utilize diamond for infrared (IR) radiation detection. To understand the fundamentals of the thermal response of diamond, Temperature Coefficient of Resistance (TCR) measurements were performed on diamond Schottky diodes which are a candidate for high temperature sensors. As a result, very high TCR values in combination with a low noise constant ($K_{1/f}$) was observed.

Keywords: Single crystal diamond, carrier transport, CVD diamond, time-of-flight, mobility, IR detector, compensation, diamond diode, drift velocity, thermal detector

Saman Majdi, Uppsala University, Disciplinary Domain of Science and Technology, Box 256, SE-751 05 Uppsala, Sweden.

© Saman Majdi 2012

ISSN 1651-6214
ISBN 978-91-554-8391-3
urn:nbn:se:uu:diva-173599 (http://urn.kb.se/resolve?urn=urn:nbn:se:uu:diva-173599)

To my wonderful Family

List of Papers

This thesis is based on the following papers, which are referred to in the text by their Roman numerals.

I M. Gabrysch, **S. Majdi**, A. Hallén, M. Linnarsson, A. Schöner, D. J. Twitchen and J. Isberg, *Compensation in boron-doped CVD diamond*, Physica Status Solidi (a) **205** (9), 2190-2194 (2008).

II **S. Majdi**, M. Gabrysch, R. Balmer, D. Twitchen, A. Tajani and J. Isberg, *Characterization by internal photoemission spectroscopy of single-crystal CVD diamond Schottky barrier diodes*, Journal of Electronic Materials, **39**, 8, 1203-1208 (2010).

III J. Isberg, **S. Majdi**, M. Gabrysch, I. Friel and R.S. Balmer, *A lateral time-of-flight system for charge transport studies*, Diamond & Related Materials **18**, 1163–1166 (2009).

IV M. Gabrysch, **S. Majdi**, D. J. Twitchen and J. Isberg, *Electron and hole drift velocity in CVD diamond*, Journal of Applied Physics **109**, 063719 (2011).

V J. Isberg, M. Gabrysch, **S. Majdi** and D. J. Twitchen, *Negative electron mobility in diamond*, Applied Physics Letters **100**, 172103 (2012).

VI **S. Majdi**, K. K. Kovi, J. Hammersberg and J. Isberg, *Low temperature hole transport in single crystal synthetic diamond*, submitted to Physical Review B, April 2012.

VII **S. Majdi**, M. Kolahdouz, M. Moeen, A. Jamshidi, R. S. Balmer, K. K. Kovi, H. H. Radamson, J. Isberg, *High performance temperature sensors using SC-CVD diamond Schottky diodes*, submitted to Applied Physics Letters, April, 2012.

Reprints were made with permission from the respective publishers.

Related contributions resulting from this work but not included in the thesis:

- VIII J. Isberg, M. Gabrysch, **S. Majdi**, K. K. Kovi and D. J. Twitchen, *On the transition between space-charge-free and space-charge limited conduction in diamond*, Solid State Sciences **13**, 1065-1067 (2011).
- IX K. K. Kovi, **S. Majdi**, M. Gabrysch, I. Friel, R. Balmer and J. Isberg, *Time-of-flight characterization of single-crystalline CVD diamond with different surface passivation layers*, MRS proceedings (2011) volume **1282**, mrsf10-1282-a09-01.
- X K. K. Kovi, **S. Majdi**, M. Gabrysch, R. Balmer and J. Isberg, *Surface passivation of single-crystalline CVD diamond by silicon oxide*, submitted to Diamond & Related Materials.
- XI R.S. Balmer, I. Friel, S. Hepplestone, J. Isberg, K-B. Lee, M.L. Markham, N.L. Palmer, J. Pilkington, **S. Majdi**, M.J. Uren, *Transport behaviour of holes in boron delta-doped diamond structures*, Submitted to IEEE Transactions on Electron Devices.
- XII M. Ullah, E. Ahmed, M. Ali, K. Welch, **S. Majdi**, N. R. Khalid, M. Ahmad, *Growth of nitrogen-incorporated diamond films using hot-filament chemical vapor deposition technique*, AMSE 2012, submitted to Advanced Science Letters (ISSN: 1936-6612).

Contents

1 Introduction........11
1.1 Diamond lattice structure........11
1.2 Types of diamonds........12
1.3 Applications........13

2 CVD Diamond........15
2.1 Growth process........15
2.2 Impurities and doping........17
2.2.1 *p*-type doping........17
2.2.2 *n*-type doping........17

3 Sample preparation........19
3.1 Diode fabrication........19
3.2 Hall bar configuration........20

4 Characterization techniques........21
4.1 Current-voltage measurements (*I-V*)........21
4.2 Capacitance-voltage measurements (*C-V*)........21
4.3 Thermal coefficient of resistance (TCR)........22
4.4 Time-of-Flight (ToF)........22
4.5 Internal photo-emission (IPE)........24
4.6 Hall-measurements........25
4.6.1 van der Pauw........25
4.6.2 Hall bars........26
4.7 Complementary techniques........27
4.7.1 Secondary ion techniques mass spectrometry (SIMS)........27

5 Electronic properties of CVD diamond........29
5.1 Compensation in *p*-type diamond........30
5.2 Schottky barrier height........33
5.3 The principle of time-of-flight........36
5.3.1 Signal interpretation........36
5.3.2 Charge injection and mobility measurements........38
5.4 Infrared detectors........39
5.4.1 Thermal detectors (TDs)........40
5.4.2 Schottky detectors........41

6 Summary of the results 43
6.1 Compensation in boron-doped diamond 43
6.2 Lateral time-of-flight measurements on thin SC-CVD layers............44
6.3 Characterization of single crystal CVD diamond Schottky barrier diodes 46
6.4 Electron and hole drift velocity measurements in CVD diamond......47
6.5 Negative electron mobility in diamond..48
6.6 Temperature Sensors using SC-CVD Diamond Schottky Diodes......49

7 Conclusion 51

8 Summary of papers 53

9 Suggestions for future work...57
9.1 Defect investigation of SC-CVD diamond..57
9.2 δ-doped diamond 58
9.3 High voltage (HV) breakdown diodes...59

Acknowledgements..61

Svensk Sammanfattning...63

Bibliography 65

Abbreviations

AC	Alternating current
BJT	Bipolar junction transistor
CVD	Chemical vapor deposition
DC	Direct current
DOS	Density of states
DSO	Digital sampling oscilloscope
DLTS	Deep level transient spectroscopy
FCC	Face cubic center
FWHM	Full width at half maximum
HF	Hot-filament
HPHT	High-pressure high-temperature
HV	High voltage
IR	Infrared
IPE	Internal photo-emission
JFET	Junction field effect transistor
LED	Light emitting diode
LToF	Lateral time-of-flight
MP	Microwave plasma
MPER	Microwave plasma enhanced reactor
MOSFET	Metal oxide semiconductor field effect transistor
MS	Metal-semiconductor
NDM	Negative differential mobility
PC	Photocurrent
PE	Photoemission
RT	Room temperature
SC	Single crystal
SBH	Schottky barrier height
SIMS	Secondary ion mass spectrometry
TCR	Temperature coefficient of resistance
TCT	Transient current technique
TD	Thermal detector
ToF	Time-of-flight
TSC	Thermally simulated current
UV	Ultraviolet

Nomenclature

a	Lattice spacing	λ	Wavelength
A	Contact area	m^*	Effective mass
A^*	Richardson's constant	m_h^*	Effective hole mass
C	Capacitance	μ_h	Hole mobility
C_j	Depletion layer capacitance	μ_e	Electron mobility
d	Sample thickness	n	Ideality factor
e	Electron (index)	n	Free electron concentration
E	Electric field	n_i	Intrinsic carrier concentration
ε_s	Relative dielectric constant	N_A	Acceptor doping concentration
E_F	Fermi level	N_D	Donor doping concentration
E_g	Indirect bandgap energy	N_{eff}	Effective density of dopants
E_A	Acceptor ionization energy	N_V	Effective DOS in valence band
E_D	Donor ionization energy	p	Hole density
g_a	Spin degeneracy factor	Q	Total charge
h	Hole (index)	q	Elementary charge
h	Planck's constant	T	Absolute temperature
$h\upsilon$	Photon energy	t_{dr}	Drift time
i	Intrinsic	τ_h	Hole drift time
I_{noise}	Noise current	τ_{tof}	Time-of-flight
I_{signal}	Current signal	Φ_B	Schottky barrier height
I_s	Saturation current	U	Bias
I_{ph}	Photoemission current	υ_d	Drift velocity
J_R	Reverse current density	υ_{sat}	Saturation velocity
J_s	Current density	V	Bias
k_B	Boltzmann's constant	V_{bi}	Built-in potential

1 Introduction

The exceptional properties of diamond make it suitable for a variety of applications [1]. Diamond is the hardest natural material. The Mohs hardness scale, on which diamond is a '10' and corundum (sapphire) a '9', does not really do justice to its incredible hardness, as diamond is very much harder than corundum. Diamond is also the least compressible and stiffest substance. It is an exceptional thermal conductor, more than 4 times better than copper.

Diamond has an extremely low thermal expansion coefficient, is chemically inert with respect to most acids and alkalis, is transparent from the far infrared to the deep ultraviolet [2], except for an absorption band, (around $\lambda = 3$ μm) and is one of only a few materials with negative electron affinity.

Natural diamonds do not conduct electricity well, although some are outstanding semiconductors. It can burn if subjected to high temperatures in the presence of oxygen, and is amazingly dense. The brilliance and fire of a diamond are due to its high dispersion and high refractive index. It also has the highest reflectance of any transparent substance.

1.1 Diamond lattice structure

There are two stable isotopes of carbon in natural diamond, 98.9% of the natural abundance is ^{12}C and the rest is 1.1% ^{13}C. The nuclear spins are zero and one-half, respectively. The simple chemical nature of diamond allowed its substance to be determined very early [3]. The crystal structure of diamond is a face-centered cubic (FCC) lattice with a cube edge length denoted by a (Fig. 1.1). The two populated sites in the FCC lattice are separated by $a\sqrt{3}/4$ see e.g. [4].

Each carbon atom joins four other carbon atoms in regular tetrahedrons (triangular pyramids). Based on the cubic form and its highly symmetrical arrangement of atoms, diamond crystals can form into several different shapes. The most common crystal structure is the eight-sided octahedron or diamond shape. Diamond crystals can also form hexagons, dodecahedra, and combinations of these shapes.

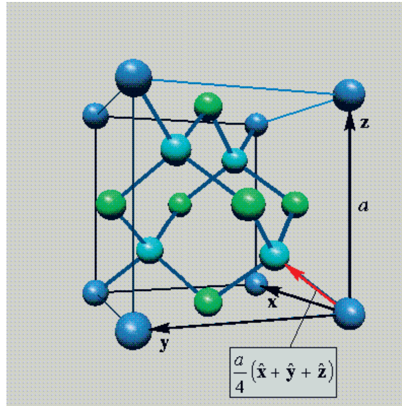

Figure 1.1 The diamond lattice (formed by the carbon atoms in a diamond crystal) consists of two interpenetrating face centered cubic Bravais lattices, displaced along the body diagonal of the cubic cell by one quarter the length of the diagonal.

1.2 Types of diamonds

From the beginning, electrical characterization of diamond was performed on natural diamond. There are four types of natural diamond (*Ia, Ib, IIa, IIb*), classified according to the presence of nitrogen in the crystal and certain other impurities. Type-*IIb* diamonds contain so little nitrogen that the crystal is a *p*-type semiconductor due to trace amounts of boron. Unfortunately, this type is very rare and expensive. To reduce the cost and increase the availability of diamond samples, synthetic methods were developed.

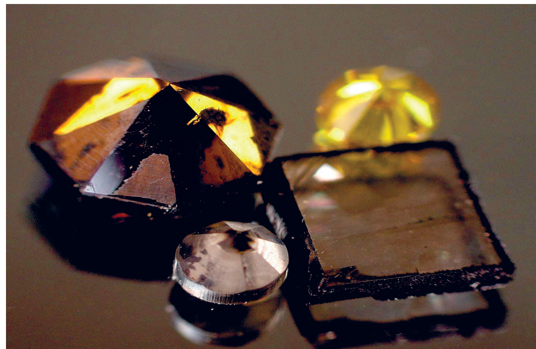

Figure 1.2 Samples of single crystal diamond grown by the CVD process.

Graphite is said to be the most stable allotrope (different forms of the same element) of carbon. Diamond exists only due to the extremely large activation barrier for conversion between itself and graphite. This metastability causes complications during diamond synthesis [5]. There are currently two main methods of synthesizing diamonds. One is the High-Pressure High-Temperature (HPHT) method where graphite is subjected to conditions similar to those under which natural diamonds are formed in the earth's mantle. In HPHT synthesis, graphite and a metallic catalyst are placed in a hydraulic press under high temperatures and pressures. The resulting diamonds are usually a few millimeters in size and too flawed for use as gemstones, but they are extremely useful as edges on cutting tools and drill-bits and for generating very high pressures in diamond anvils. The first diamond made using this process was synthesized in 1953 [6] and since then, HPHT diamonds have been available and electrically characterized.

In order to achieve diamond crystals with higher purity and less defects, another method is used, called Chemical Vapor Deposition (CVD). This deposition method was first utilized in the 1950s by Eversole [7]. Since the 1980s it is possible to synthesize diamond films with good control of the surface morphology by CVD. Initially, this method resulted in polycrystalline material but nowadays one can grow freestanding single-crystal CVD (SC-CVD) diamond of high quality. These diamond films are expected to be one of the most promising semiconducting materials and the electronic characteristics of diamond films have greatly improved.

1.3 Applications

Due to the extraordinary properties of diamond such as extreme hardness, chemical inertness, optical transparency, high thermal conductivity in combination with electrical insulation or semiconducting properties, more and more fields of application recognize the benefits provided by this material. In applications involving extremely high mechanical loads or severe abrasive conditions, diamond is often the only material that can meet the demanding requirements. High temperature electronics applications require a material for advanced semiconductor devices, which can operate where conventional silicon-based electronics cannot function. Some potential applications of CVD diamond films and related properties are listed in table 1.1.

Table 1.1 List of selected potential applications of CVD diamond.

Function	Field of application
High temperature sensors	Automobile and aircraft engines
High frequency/high power transistors	High speed transistors, Radars
High voltage transistors	Electric power control
Light emission	LEDs and lasers in UV region, white luminescence and light source for printer
X-ray windows IR windows	X-ray lithography masks and IR windows
Pressure sensing	Pressure sensor at high tempera-ture
Radiation hardness	Particle/radiation detectors

2 CVD Diamond

One of the most promising semiconducting materials, which can be used for many extreme microelectronic applications, is diamond. The excellent chemical, thermal, electrical and mechanical properties are suitable for high-power, high-temperature and high-frequency devices. But before the realization of active devices in diamond, several problems must be overcome [8, 9].

Due to the negative effect of contaminations and structural defects on the behavior of diamond [10], especially its electrical performance, it is important to grow diamond into films or substrates of single-crystal quality. In the 20th century, most of the published results have been performed on polycrystalline diamond. However, free-standing single-crystal CVD diamonds are now commercially available through companies such as *Element Six Ltd.* and the EDP corporation.

The fundamental problem of diamond synthesis is the allotropic nature of carbon. Under ordinary conditions diamond is not the thermodynamically stable crystalline phase of carbon. Hence, the main requirement of diamond CVD is to deposit carbon and simultaneously suppress the formation of graphitic sp^2-bonds. This can be realized by establishing high concentrations of non-diamond carbon etchants such as atomic hydrogen. Usually, those conditions are achieved by admixing large amounts of hydrogen to the process gas and by activating the gas either thermally or by microwaves to form plasma.

2.1 Growth process

CVD processes for diamond synthesis can be used for the growth of both single crystal and polycrystalline forms of the material. The actual conditions required for making either type of diamond are very similar; it is the choice of substrate and keeping homogenous growing conditions that determines which type will grow. For single crystal CVD diamond, a single crystal diamond substrate is required and the new diamond film grows epitaxially, with the deposited film taking the same lattice structure and orientation as those of the substrate. For polycrystalline diamond, a non-diamond substrate is normally used.

In diamond CVD synthesis, the process is generally carried out below atmospheric pressure. The CVD growth is based on the activation of a H_2/CH_4

gas mixture with a high hydrogen concentration [11]. Only a small amount of hydrocarbon (methane), often between about 1 and 5%, is normally present in the gas mixture and provides the source of carbon from which the diamond is formed. The various diamond CVD techniques differ mainly in the way of gas phase activation and dissociation. Table 2.1 summarizes the precursors and conditions needed to grow CVD diamond.

Table 2.1 An example of required growth conditions for CVD diamond films.

CH_4/H_2 (%)	0.05-0.075
Total gas pressure (kPa)	~10
Total gas flow rate (sccm)	400-1000
Substrate temperature (°C)	800-900

The first critical step of CVD diamond growth is nucleation and the control of it will decide the diamond film properties, such as transparency, grain size and roughness [12]. The most common deposition techniques are microwave plasma (MP) assisted CVD and thermally assisted CVD (Fig. 2.1), usually realized by gas activation with a hot filament (HF) (~ 2200°C). In contrast to the hot filament method, the plasma assisted growth offers uniform films over larger substrate areas with the possibility of industrial scale-up by using more powerful reactors.

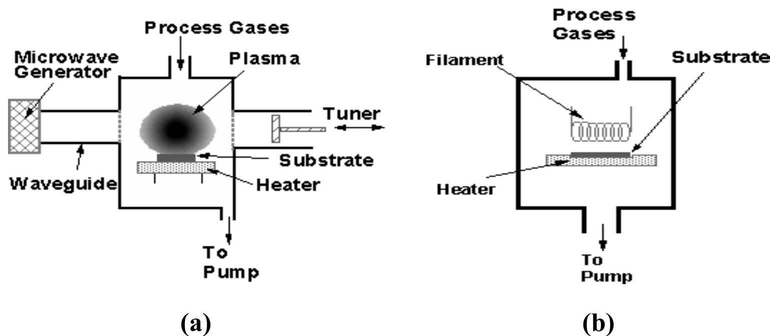

Figure 2.1 The most common types of low pressure CVD reactors. (a) Microwave Plasma Enhanced Reactor (MPER), (b) Hot filament reactor.

2.2 Impurities and doping

Diamond with its wide bandgap normally behaves as an insulator at room-temperature. The superior properties of diamond make it desirable to be used as a semiconductor, and it is therefore necessary to introduce shallow donors or acceptors into the material. To achieve high activation in a doped semiconductor it is necessary to have a low degree of compensation. This puts a high demand on the achievement of a controlled doping process.

There are several substances which can be used as impurities in diamond. Hydrogen (H) related defects are very complex and exist due to the hydrogen-rich growth atmosphere. The passivation effect of hydrogen on diamond dopants has been investigated thoroughly [13, 14]. Silicon (Si) and sulfur (S) are two other elements which are common impurities in diamond. These are often unintentionally introduced into diamond during the growth process. Silicon is centered deep in the bandgap, having an ionization energy of 2 eV [15]. In the case of sulfur this value is not very well known and varies significantly (0.77 eV [16] – 1.4 eV [17]).

These impurities are located deep in the bandgap and do not act as dopants in diamond at room temperature. Other impurities which can be used as dopants, the *p*-type boron (B) and *n*-type phosphorus (P) are described in following sections.

2.2.1 *p*-type doping

p-type diamonds containing boron exist naturally in type *IIb* natural diamonds. Boron can easily be incorporated substitutionally into the diamond lattice during the CVD process [18]. This can e.g. be done by adding diborane B_2H_6 into the gas mixture.

A low boron concentration creates an acceptor level with an activation energy of 0.37 eV [19] and transforms insulating diamond into a *p*-type semiconductor. At a higher boron concentration, diamond shows metallic properties due to the broadening of the acceptor level into a band [20]. Recent reports have shown a superconducting behavior in heavily boron doped diamond below 11 K [21]. This observation seems to be related to the strong electron-phonon coupling in diamond [22].

2.2.2 *n*-type doping

The majority of diamond samples used for optical and electrical studies are *p*-type diamonds, despite the fact that the most common impurities in natural diamond are *n*-type (type *Ib* diamonds).

Nitrogen and phosphorus are candidates to act as a donor. They can easily replace carbon and fit substitutionally into the diamond crystal. However, nitrogen induces a deep energy level, 1.7 eV below the conduction band

minimum. Unfortunately, this deep level does not donate significant numbers of electrons to the conduction band at room temperature [23].

Phosphorus, an element in group V, has proven to be an interesting donor in diamond, despite the rather deep level, 0.52 eV in the bandgap [24]. Fig. 2.2 shows the position of the common doping elements and their energy levels inside the diamond bandgap. An early attempt to dope diamond with phosphorus by the CVD technique, turned out to be difficult with rather poor electrical performance. Today it is possible to grow both polycrystalline diamond by heteroepitaxy and homoepitaxial high quality P-doped diamonds with electron mobilities up to 660 $cm^2 V^{-1} s^{-1}$ [25]. High doping concentrations can be achieved by growing in the <111> crystallographic direction [26-27].

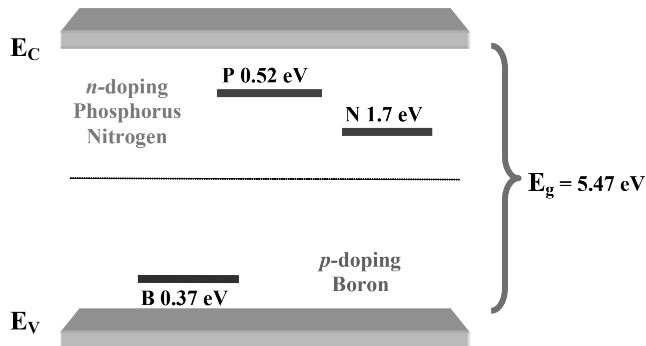

Figure 2.2 Boron, nitrogen and phosphorus ionization energies in CVD diamond.

3 Sample preparation

The samples described in **Papers I-VII** were synthesized by *Element Six Ltd.* by CVD, first described in [28]. Initially, homoepitaxial boron-doped CVD diamond layers were deposited onto specially prepared high-pressure, high-temperature grown synthetic diamond substrates using a diborane (B_2H_6) addition to the $H_2/CH_4/Ar$ source gas mixture. A further CVD layer grown under conditions of high purity was deposited on this doped CVD material. The HPHT substrates were subsequently removed by laser cutting.

3.1 Diode fabrication

Before metallization, the samples were treated in a graphite etch (HNO_3:$HClO_4$:H_2SO_4) up to 200°C and the surfaces were oxygen terminated in a mild oxygen plasma. To form an ohmic back contact for *I-V*, *C-V*, *I-T* and time-of-flight (ToF) measurements, metal contacts were deposited on the boron doped material under high vacuum (10^{-7} Torr) in a Von Ardenne CS 730 Magnetron sputter. Circular Schottky contacts were formed on the top side of the samples (see Fig. 3.1). Gold (Au) contacts were deposited by sputtering using a K675XD Turbo Sputter Coater. Nickel (Ni) and aluminum (Al) contacts were deposited using a Von Ardenne CS 730 Magnetron sputter in high vacuum (10^{-7} Torr). To pattern the contacts, standard optical lithography and wet chemical etching were used. In the time-of-flight characterization techniques (vertical and lateral), the same sequences of processing steps (except for the choice of metal) were used to prepare the samples.

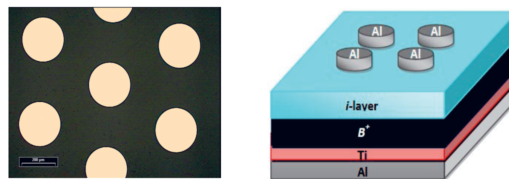

Figure 3.1 Fabrication of the Schottky contacts on SC-CVD diamond.

To measure internal photoemission, semitransparent Schottky contacts (10-15 nm of Au, Al and Ni) were patterned on the top surface of the samples, while ohmic back contacts were deposited in the manner previously described.

3.2 Hall bar configuration

A lift-off process was applied to fabricate Hall bars on delta-doped diamond samples (8-10 nm thick delta-layers). A standard optical lithography process was performed to transfer the pattern to the sample. Aluminum contacts were deposited using a Von Ardenne CS 730 Magnetron sputter in high vacuum (10^{-7} Torr) to form a protection mask during the etching of the diamond surface. The samples were etched using a dry etch process in a commercial Inductively Coupled Plasma (ICP) Plasma Therm SLR system by introducing Ar/O_2 gas. A 50 nm etching depth was chosen in order to etch through the delta-layer and reach the intrinsic bulk. Finally, through a second step of photolithography and ICP the aluminum mask was removed and the Hall bars were formed. The thickness and topography of the Hall bars were investigated using a profilometer (Fig. 3.2).

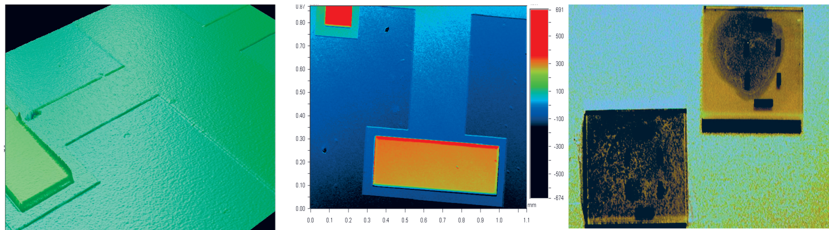

Figure 3.2 Topographic view of a Hall bar fabricated on CVD diamond taken by a Vecco profilometer and two SC-CVD diamond samples with the Hall bar.

4 Characterization techniques

In this work several characterization techniques have been utilized to study single-crystal CVD diamond's electrical properties. The main techniques used are: Time-of-flight (ToF), internal photo-emission (IPE), current-voltage measurements (*I-V*), capacitance-voltage measurements (*C-V*), thermal coefficient resistance (TCR) and Hall measurements. In addition, secondary ion mass spectrometry (SIMS) is described which was used to determine doping levels.

4.1 Current-voltage measurements (*I-V*)

Current-voltage measurements allow an estimation of the leakage current characteristics and the critical breakdown field of a dielectric. Study of the *I-V* measurements at different temperatures allows better understanding of the origin of the leakage current. The characterizations were performed on Schottky metal contacts without an edge-termination on both *p*-type material (*p*) and *p*-type material with a thin intrinsic overlayer (*i-p*).

Forward *I–V* measurements were performed on several diodes on each sample at room temperature to investigate the homogeneity of the doping. A Keithley 6485 picoamperemeter in combination with a Keithley 2400 sourcemeter was used to measure the *I-V* characteristics of these diodes which were placed on a hotplate that can achieve temperatures in the interval 300-600 K.

4.2 Capacitance-voltage measurements (*C-V*)

Capacitance-voltage measurements are widely used to determine semiconductor parameters, particularly of MOSFET structures. However, other types of semiconductor devices can also be characterized by *C-V* measurements, including bipolar junction transistors (BJTs), JFETs, III-V compound devices, photovoltaic cells, among many others.

A *C-V* measurement of semiconductors devices and interfaces is a very sensitive and powerful technique for electrical characterization. It is based on monitoring the capacitance for a fixed DC voltage. In addition to the Hall-effect measurements, capacitance-voltage measurements were per-

formed to get a different measurement of the effective doping concentration. The measurements were made using a Signal Recovery 7280 wide-bandwidth lock-in amplifier. The bias was applied using a Keithley 2400 sourcemeter.

4.3 Thermal coefficient of resistance (TCR)

In order to analyze the two most important parameters, thermal coefficient of resistance (TCR) and signal-to-noise ratio, for a high performance bolometer, a study was carried out in collaboration with colleagues at KTH, Stockholm (**Paper VII**). Here, both *p*-type material and *p*-type material with a thin intrinsic layer on top were used to form Schottky diodes.

TCR measurements were performed using a Cascade 11000 shielded probe station with a temperature-controlled chuck. The noise voltage of the device was measured using a battery powered low-noise preamplifier and a HP49810 vector spectrum analyzer was used. The sample surface temperature was double-checked by a laser interferometer to enhance the accuracy of the experiment. Temperatures in the interval 300-600 K were applied.

4.4 Time-of-Flight (ToF)

Hall-effect measurements are generally used to measure the mobilities of the charge carriers in semiconductors. However, there are some difficulties to utilize this technique on highly resistive wide bandgap semiconductors, such as intrinsic diamond. To overcome this, the time-of-flight (ToF) technique, also called the transient current technique (TCT) can be used. With this technique, it is possible to investigate many important electrical properties of semiconductors, such as carrier drift mobility, charge collection and trapping lifetimes. In order to create electron-hole pairs in intrinsic diamond, several methods such as pulsed electron beam [29], pulsed X-ray [30], α-particles [31] and UV-pulsed laser [28, 32-33] have been used. The time-of-flight technique allows investigation of the carrier transport through the diamond crystal (vertically) by preparing the sample in the following configuration:

- Deposition of a transparent net-contact (Au, Al or Ni) on one side of the sample followed by a backside (Ti/Al) contact. This is shown in Fig. 4.1 and it is suitable for bulk studies.

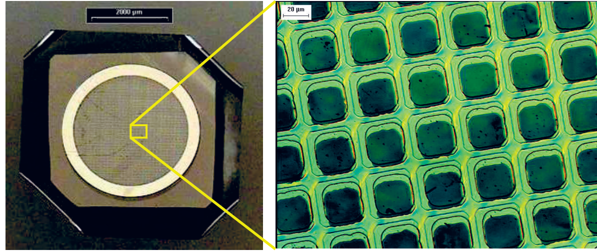

Figure 4.1 Deposited semitransparent contact on CVD Diamond.

The semitransparent contact makes it possible to apply both a relatively homogenous electric field and to create electron-hole pairs within the vicinity (a few micrometers) of the illuminated side of the sample due to the strong absorption process. The time-of-flight in our lab uses a short (3 ns FWHM) UV pulsed laser (Nd-YAG laser) with a pulse of 213 nm wavelength produced at a 10 Hz repetition rate. A maximal intensity of 18 mJ can be achieved. The samples were mounted in a LCC ceramic chip carrier and placed in a liquid helium (LHe) cooled Janis ST-300MS vacuum cryostat. The temperature was monitored using a Lakeshore 331 temperature controller with a calibrated TG-120-CU-HT-1.4H GaAlAs diode sensor in good thermal contact with the sample.

The carrier transport measurements can also be performed along the surface (laterally) with the sample in the following configuration:

- Deposition of two parallel electrodes (metal contact made by Au, Al or Ni) on the same side of the sample. This configuration is shown in Fig. 4.2 and it has been formed on samples for lateral time-of-flight (LToF) studies.

Figure 4.2 Deposited lateral contacts on CVD Diamond.

This configuration has allowed us to analyze transport characteristics of thin layer diamond films and delta-doped structures. The intensity can be controlled by several interference and attenuation filters. To ensure capacitive voltage division and avoid charging of the sample, the bias voltage was applied in pulses of 50 µs duration. In case of (LToF) a cylindrical square lens is used in conjunction with reflective optics to focus the beam into a line on the sample, see Fig. 4.3. A CCD camera is used to view the position of the focused beam.

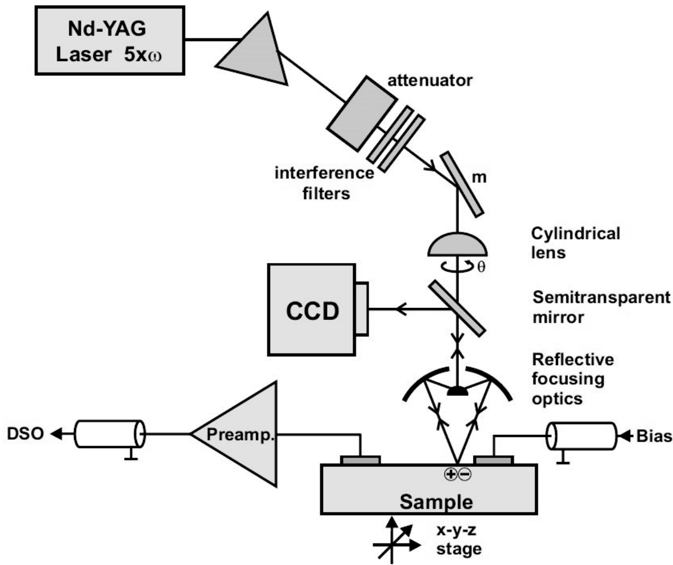

Figure 4.3 Schematic of the LToF setup. The sample is illuminated with 3 ns (FWHM) 213 nm UV light from a quintupled Nd-YAG laser.

4.5 Internal photo-emission (IPE)

IPE is defined as an optically induced transition of a mobile charge carrier across the interface between two solid phases, one is the emitter and the other is the collector. Light is directed onto a sample, where it is absorbed and imparts excess energy into the material in a process called photo-excitation.

For the IPE measurements described in **Paper II,** a halogen filament lamp attached to an Acton Research SP150 blazed grating monochromator was used to illuminate diodes. A sharp cut-off colored glass filter mounted between the lamp and the monochromator was used to eliminate higher orders from the grating. A Newport 818-BB-22 photodetector with well known photoresponsivity was used to measure the intensity vs. the wavelength vari-

ation of the entire optical setup (lamp + filter + monochromator + fibre). The diamond diode current was measured with a Keithley 6485 picoamperemeter.

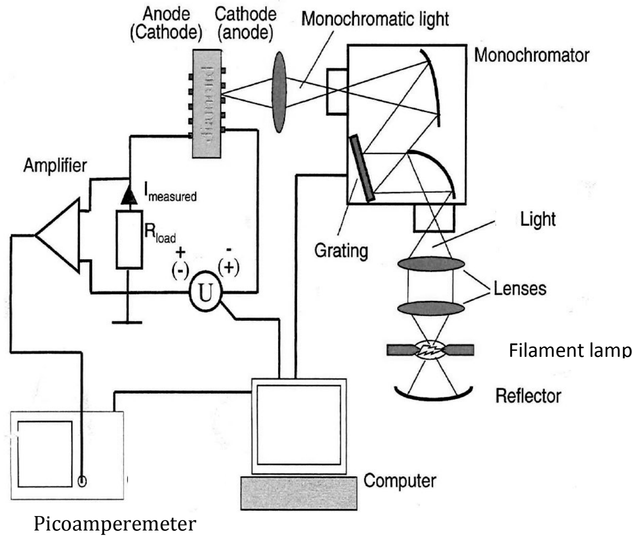

Figure 4.4 Schematic of the photocurrent setup used to obtain SBH data.

4.6 Hall-measurements

The key feature of Hall-measurements is the ability to determine the carrier density, the carrier type and the carrier concentration. By forming either van der Pauw contacts or Hall bars and measuring the resistivity and Hall voltage of the sample it is possible to extract the carrier mobility with a relatively simple measurement. Variable temperature Hall effect measurements were made using two systems: van der Pauw and in particular Hall bar.

4.6.1 van der Pauw

The van der Pauw structure is probably the most popular and simplest Hall measurement geometry. Nevertheless, some requirements need to be fulfilled before one can calculate the above-mentioned parameters (e.g. sufficiently small contacts and uniform sample thickness). To determine the doping/drift parameters and degree of dopant compensation in **Paper I,** Hall-measurements were made using the van der Pauw configuration. The electrodes were formed at the four corners of each sample by ion implantation of

boron. Hall-effect measurements were made in the temperature range of 80-450K in a magnetic field of 0.5 T.

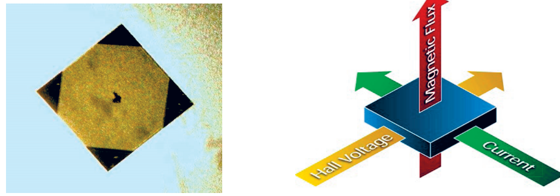

Figure 4.5 A diamond sample with a van der Pauw configuration and a schematic diagram of the Hall-effect. Current and a perpendicular magnetic field create a potential difference perpendicular to both the current and the magnetic field.

4.6.2 Hall bars

The Hall bar is a good geometry for making resistance measurements. For this reason, Hall bars of similar geometries are commonly used when measuring Hall mobility on samples with low resistances. Recently, a polarity-switched AC Hall system using a 0.5 T magnet was installed at the Ångström laboratory.

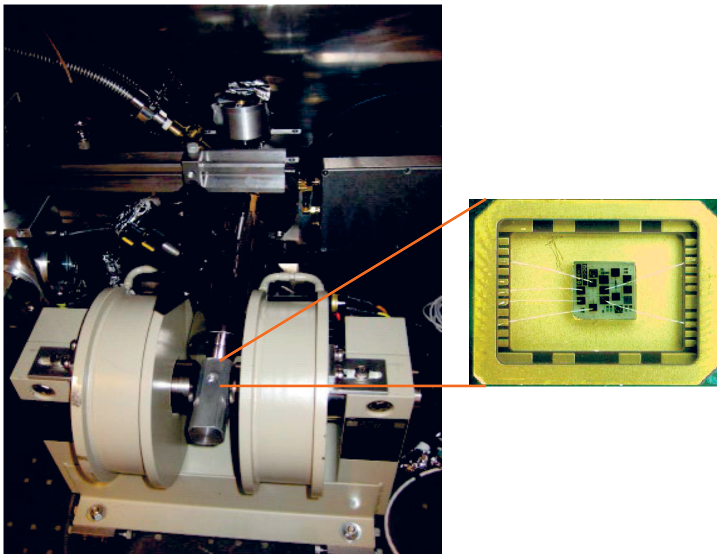

Figure 4.6 Electromagnet and cryostat in the Hall setup (left). LCC package used for mounting the Hall bar diamond sample (right).

The system in Fig. 4.6 is computer controlled and the measurement is fully automated. The switching is done using a Keithley model 7065 Hall effect card. The current and voltage is measured using two Signal recovery 7265 lock-in amplifiers. The samples are wire bonded on a LCC cavity package, placed with 90° rotation in the customized Janis ST-300MS vacuum cryostat mentioned in section 4.4. A magnetic field is applied using a GMW 3470 water-cooled electromagnet and the field strength was measured by a Sypris 7010 Gaussmeter. A calibrated TG-120-CU-HT-1.4H GaAlAs diode measures the sample temperature and a Lakeshore 331S temperature controller is used to keep the temperature constant. The applicable temperature in this system is in the range of 4 - 450 K, using liquid helium or liquid nitrogen for cooling.

4.7 Complementary techniques

4.7.1 Secondary ion techniques mass spectrometry (SIMS)

Secondary ion mass spectrometry is used to obtain accurate measurements of dopant and impurities. Due to its unique capabilities of high detection sensitivity for a variety of elements, SIMS is an essential tool for characterization of impurities in semiconductor materials.

SIMS measurements were performed (**Paper I**) on homoepitaxial highly boron-doped CVD diamond samples, using a Cameca ims 4f micro-analyzer. A sputtering beam of 8.2 keV $(O_2)^+$ ions was rastered over an area of 200 × 200 μm^2 and secondary ions of B^+ were collected from the central region (~60 μm). In order to minimize the effect of sample charging, electron flooding was employed. The erosion rate was typically 10-20 Ås^{-1} as determined by the crater depth measurements using a KLA-Tencor P15 profilometer.

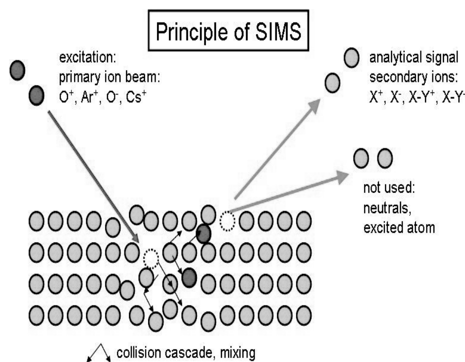

Figure 4.7 The principle of secondary ion mass spectrometry.

5 Electronic properties of CVD diamond

Diamond has long been considered to be an exceptional material for the fabrication of active electronic devices for the most demanding high-power and high-frequency applications. However, until recently it has not been available in sufficient quality or purity. Theoretical studies indicate that CVD diamond could offer a substantially higher level of performance than other established electronic materials, such as silicon or gallium arsenide in many applications. Due to the large bandgap and material purity, diamond is an excellent electrical insulator. By doping, however, CVD diamond can be made conducting.

Diamond is a wide bandgap semiconductor with a 5.47 eV indirect bandgap at 300 K. The highest drift mobility measured has been reported by Isberg *et al*. [28] and is 4500 cm^2/Vs for electrons and 3800 cm^2/Vs for holes. These are much higher than the mobilities of widely used conventional semiconductor materials, such as Silicon (1450 cm^2/Vs for electron mobility and 480 cm^2/Vs for hole mobility) and other wide bandgap materials, such as Silicon carbide (SiC) (900 cm^2/Vs for electrons and 120 cm^2/Vs for holes) and Gallium nitride (GaN) (2000 cm^2/Vs for electrons and 200 cm^2/Vs for holes). Diamond has a very high electric breakdown field (20 MV/cm) [34] and a high carrier saturation drift velocity (2.7×10^7 cm/s for electrons and 1.4×10^7 cm/s for holes) [35]. Room-temperature values of up to 24 W/cm K for the thermal conductivity have been reported [36]. The resistivity can exceed 10^{16} Ω cm [37] in pure diamond.

This chapter focuses on some of the basic theory behind electrical transport, carrier concentration dependence on the doping density, determination of Schottky barrier height and heat effected resistance sensitivity in single-crystal CVD diamond.

5.1 Compensation in *p*-type diamond

Many of the extreme properties of diamond can be explained by looking at the crystal structure of diamond. Other parameters such as mobility depend on factors like concentration of extrinsic contaminations and dopants or intrinsic defects (**Paper I**).

These defects and impurities exist in all semiconductors and even in very pure diamond crystals. Obviously, in order to have any kind of conductivity, a reasonable amount of dopants is needed which can be introduced during growth or ion-implanted into the sample. During these processes it is inevitable to introduce undesirable levels into the bandgap which will affect the performance of the device either by compensation or reduced carrier lifetime.

The relatively deep energy level of boron in the bandgap (0.37 eV) leads to a low activation at room-temperature (RT). The high activation energy is the reason for a strong temperature dependence of the carrier concentration. Because of the low activation it is important to keep the ratio between the dopants and the compensating defect concentration at a low level.

Volume fractions lower than 10^{-3} between the compensating donor (N_D) and the acceptor concentration (N_A) must be obtained to achieve diamond devices with high performance.

Several mechanisms affect the carrier transport in a semiconductor [38]. At low temperature, the main carrier transport in a *p*-type CVD diamond is dominated by a tunneling process called hopping conduction [37]. The process is quite slow and the mobility is also significantly low. This phenomenon was observed in **Paper I,** by Hall-measurements in a low temperature range of (80-150 K). In an extrinsic semiconductor, the difference in the concentration of donors and acceptors gives the effective density, N_{eff}.

$$N_{eff} = N_A - N_D \tag{5.1}$$

If we consider a *p*-doped wide bandgap semiconductor, such as boron doped diamond, where $N_A > N_D$ the hole concentration p can be calculated from:

$$\frac{p(p + N_D) - n_i^2}{N_A - N_D - p - n_i^2 / p} = \frac{N_V}{g_a} \exp(-E_A / k_B T) \tag{5.2}$$

where n_i, N_V, E_A, k_B, T and g_a are the intrinsic carrier concentration, the valence band effective density of states, the acceptor ionization energy, the Boltzmann constant, the absolute temperature and the spin degeneracy factor for the valence band, respectively. The latter is expected to follow Eq. 5.3 which is valid in case of a non-degenerate semiconductor [39]:

$$g_a = 4 + 2\exp(-\Delta / k_B T) \tag{5.3}$$

where Δ equals to spin-orbit branch, split off energy [40]. For temperatures below 1000 K, due to the wide bandgap of diamond, the intrinsic concentration, n_i can be neglected. N_V, which represents the weighted sum of all states in the valence band, has the following temperature dependence:

$$N_V = 2\left(\frac{2\pi\, m_h^* k_B T}{h^2}\right)^{3/2} \tag{5.4}$$

where m_h* is the density of states effective hole mass. The carrier concentrations N_A and N_D and acceptor ionization energy E_A were obtained using Eq. (5.5) and performing a least-squares fit in the upper temperature range of the measured hole concentration data, by making the assumption that n_i is negligible in Eq. (5.2).

$$p = \sqrt{\left(\frac{N'_V + N_D}{2}\right)^2 + N'_V\left(N_A - N_D\right)} - \frac{N'_V + N_D}{2} \tag{5.5}$$

Here, N'_V is the right side of Eq. (5.2) and shows explicit temperature dependence.

$$N'_V = \frac{2}{g_a}\left(\frac{2\pi\, m_h^* k_B T}{h^2}\right)^{3/2} \exp(-E_A / k_B T). \tag{5.6}$$

The interaction of the carrier concentration exhibits different behaviors in a compensated *p*-type diamond for the temperature interval shown in Fig. 5.1.

i. For low temperatures, when $p << N_D$, $p << N_A - N_D$ and $p >> n_i$, we obtain:

$$p = \frac{N_A - N_D}{N_D} \cdot \frac{N_V}{g_a} \exp(\frac{-E_A}{k_B T}) \tag{5.7}$$

Here the donor is partially compensated and the acceptor is incompletely ionized.

ii. For intermediate temperatures, when $p >> n_i$ and $N_A >> p >> N_D$

$$p = \sqrt{(N_A - N_D)\frac{N_V}{g_a}} \cdot \exp(\frac{-E_A}{2k_BT}) \tag{5.8}$$

iii. For high temperatures, when $E_A > k_BT$ and $p >> n_i$

$$p \equiv N_{eff} = N_A - N_D \tag{5.9}$$

At this point the temperature dependency of the carrier concentration is negligible. For even higher temperature intervals (iv), the intrinsic region, where $p \approx n_i$ is reached.

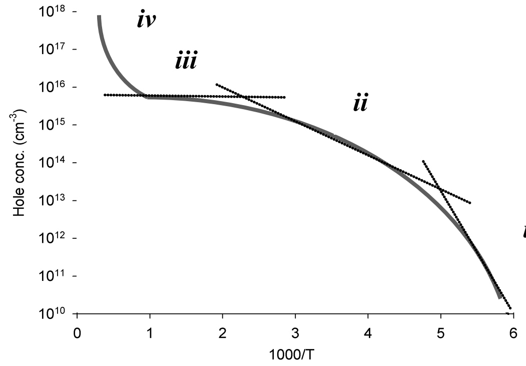

Figure 5.1 Typical behavior of the hole concentration as function of inverse temperature for CVD diamond.

The effective carrier density can be obtained from *C-V* measurements on Schottky diodes. By fitting experimental data to Eq. (5.10) it is possible to determine the effective density (N_A - N_D).

$$\frac{1}{C_j^2} = \frac{2(V_{bi} - V)}{q\varepsilon_S(N_A - N_D)} \tag{5.10}$$

where C_j is the junction depletion layer capacitance per unit area, V_{bi} the built-in potential and $\varepsilon_S = 5.7\varepsilon_0$ the permittivity of diamond.

5.2 Schottky barrier height

One of the most important properties of a metal-semiconductor (MS) interface is its Schottky barrier height (SBH). The SBH is the rectifying barrier for electrical conduction across the MS junction and, therefore, it is of great importance for the desired operation of any MS device. The magnitude of the SBH reflects the mismatch in the energy position of the majority carrier band edge of the semiconductor and the metal Fermi level, across the MS interface. The requirements for achieving high-voltage high-power switching devices are low forward losses, i.e. small threshold voltages, but also high reverse blocking voltages [41]. Ideally, for a *p*-type interface, the SBH is the difference between the valence band maximum of the semiconductor and the metal Fermi level. The Schottky barrier height has an influence on the leakage current and the breakdown voltage. This makes it an important parameter for adjusting the trade-off between low forward losses and high breakdown voltage in Schottky diodes.

Several methods can be use to determine the SBH. In **Paper II** photoemission, *I-V* and *I-T* measurements have been performed to obtain information on the SBH.

Internal photo-emission

Internal photo-emission (IPE) measurements were performed to determine the SBH. In this method the energy band offset at the interface is associated with the threshold determined as the minimal photon energy necessary for injection of a charge carrier. Unlike the *C-V* and *I-V* techniques that are often used to measure the barrier heights, the internal photoemission technique is not as sensitive to problems related to leakage currents, series resistance, thin interfacial layers, deep traps, and ideality factors and so it should in principle provide a more accurate measurement of the barrier height.

For photon energies slightly exceeding the barrier height, $hv > \Phi_B$, the yield Y defined as the ratio of the photocurrent I_{ph} to the photon flux is expected to follow the Fowler law and it is given by Eq. (5.11) [42].

$$Y \propto (hv - q\phi_{\mathbf{B}})^2 \tag{5.11}$$

Extrapolation of the linear region to zero $Y^{1/2}$ in a Fowler plot ($Y^{1/2}$ vs. photon energy hv) extracts the SBH and this is visualized in Fig. 5.2.

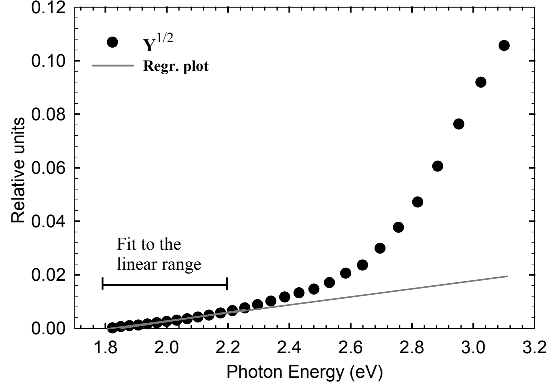

Figure 5.2 A typical Fowler plot and the linear regression region.

Current-voltage

To calculate the barrier height, the reverse saturation current density $J_s = I_s/A$ was obtained by extrapolation of the forward characteristic at zero bias voltage. To investigate the homogeneity of the doping, *I-V* measurements were performed at room temperature. The thermionic current-voltage relationship of a Schottky barrier diode, neglecting series and shunt resistance [43], is given by:

$$I = I_S(\exp(\frac{qV}{nk_BT}) - 1) \tag{5.12}$$

where

$$I_S = AA^*T^2 \exp(\frac{-q\phi_B}{k_BT}) \tag{5.13}$$

and

$$A^* = \frac{4\pi q k_B{}^2 m^*}{h^3} = 120\left(\frac{m^*}{m_0}\right) \text{A cm}^{-2}\ \text{K}^{-2} \tag{5.14}$$

Where A is the diode area, T the absolute temperature, n the ideality factor, I_S the saturation current, $m*$ the effective mass and $A*$ the Richardson's constant. The Schottky barrier height is denoted by Φ_B.

Current-temperature

In general defects might cause thermal activation of the reverse leakage. Due to this phenomenon it is important to study the current at different temperatures to achieve a better evaluation of the SBH. By assuming that the ideality factor n is known (the result from the *I-V* fit can be used) one can determine SBH from the slope of a (Richardson) plot where ln $(1/T^2)$ is plotted versus

$1/T$ at a constant forward bias. For $V >> k_BT/q$, Eq. (5.12) and (5.13) can be written as:

$$\ln\left(I/T^2\right) = \ln\left(AA^*\right) - \frac{q(\phi_B - V/n)}{k_BT} \tag{5.15}$$

The barrier height is then given by:

$$\phi_B = \frac{V}{n} - \frac{k_B}{q}\frac{\partial\left[\ln\left(I/T^2\right)\right]}{\partial(1/T)} \tag{5.16}$$

In the current-temperature measurement, the voltage is fixed and the temperature is varied. Extraction of the SBH from the temperature dependence of the forward current density of a diode is determined by a linear fit to the data.

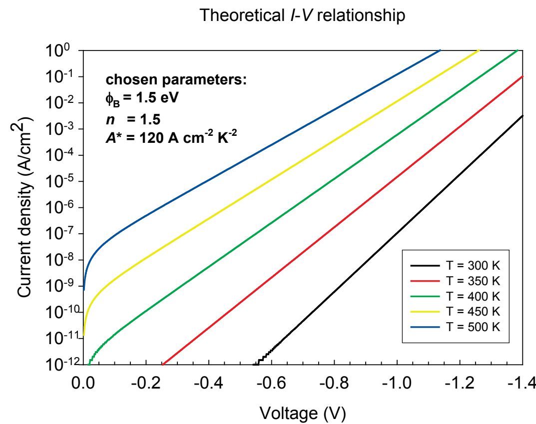

Figure 5.3 Theoretical *I-V* relationships for a *p*-type semiconductor at five different temperatures.

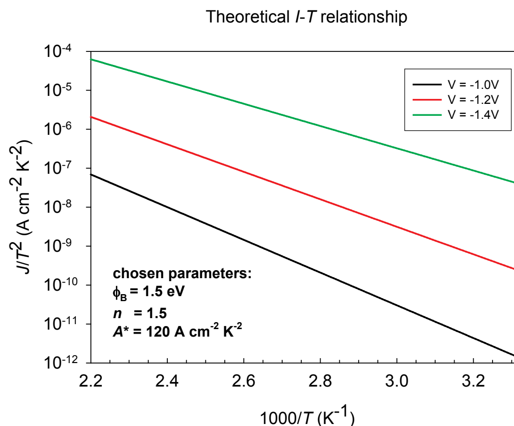

Figure 5.4 Theoretical *I-T* relationships for a *p*-type semiconductor at three different voltages.

5.3 The principle of time-of-flight

In comparison to polycrystalline diamond, single crystal diamond (SC-CVD) offers important advantages for applications in electronics and radiation detection. This is because SC-CVD diamond exhibits superior charge transport characteristics, in particular high drifts mobility and extended charge carrier lifetime. So far, only limited studies have dealt with the measurements of electrical transport parameters in SC-CVD diamond.

In ToF electron-hole pairs are generated using ionized radiation with sufficient energy. The radiation intensity should preferably be low to avoid space-charge effects. The main principle is to create electron-hole pairs in the sample, and to analyze the resulting current pulse from drifting charges in an applied field measured at a contact at a distance *d* from the injection point. Due to the wide bandgap of diamond (5.47 eV) we use a 213 nm UV-pulsed laser to illuminate the sample. This provides the photon energy necessary to create electron-hole pairs.

In **Paper III** we describe a system that has been built to study the carrier transport between two metal electrodes at certain distance on one side of a sample (Lateral alignment). The main purpose is to analyze electrical transport properties of thin intrinsic diamond films.

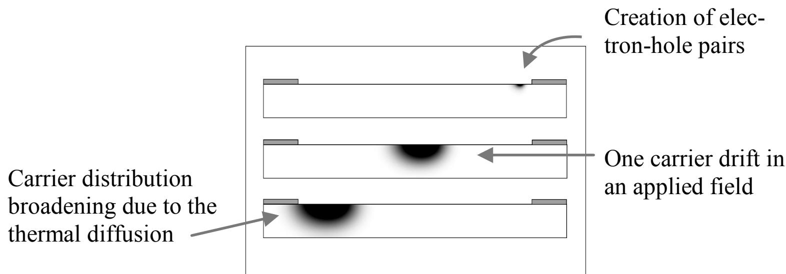

Figure 5.5 Device simulation of a carrier transit, showing the hole concentration at three different times.

Furthermore, temperature dependent ToF measurements can provide information about the charge carrier scattering mechanisms dominating the charge transport.

5.3.1 Signal interpretation

By applying an electric field the electrons and holes begin to drift towards the anode and the cathode respectively. As soon as the charge carriers begin their motion, they induce a current. The ToF technique measures the dura-

tion of the current pulse induced by the drift of charge carriers, under the influence of the field.

The current pulse width equals the time the charge carriers need to traverse the detector (t_{dr}) under the assumption that the effective charge carrier lifetime (τ) is longer than the drift time. Depending on the direction of the electric field, one polarity of charge carrier drifts across the whole detector thickness while the other polarity carrier only drifts a short distance.

Simulation of the output signal was carried out to obtain an analysis method. The expression below is an approximation of the induced current by the laser, where α and β are constants [44].

$$I(t) = \alpha \cdot \left(1 + \mathrm{erf}\left(\frac{t - t_0}{\sigma_0}\right)\right)\left(1 + \mathrm{erf}\left(\frac{t_1 - t}{\sigma_1}\right)\right)\exp(\gamma t) + \\ + \beta \cdot \exp\left(-\left(\frac{t - t_0}{\sigma_0}\right)^2\right) \tag{5.17}$$

Processes such as photoelectric effect and plasma relaxation, which are shorter than the laser pulse duration, are taken into account by the last term in Eq. (5.17). The generation and extraction of charge is described by the two 1+erf (*) factors in the equation.

The effect of a homogeneous distributed space charge on the applied field and the extracted charge by the trapping or recombination are described by the exp(γt) factor. Fig. 5.6 shows example of fits, derived from Eq. (5.17) and current data obtained from experimental measurements.

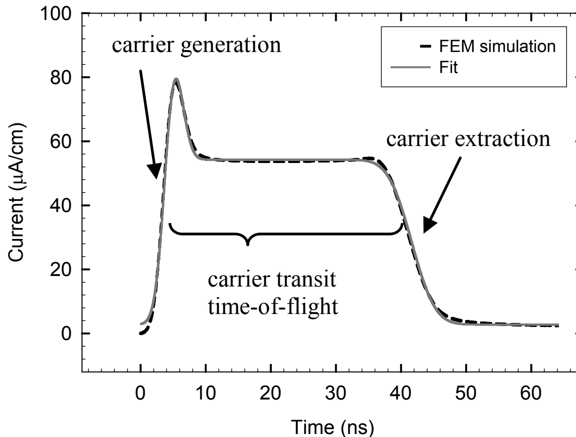

Figure 5.6 Example of fit of expression (5.17) to current calculated in a device simulation.

5.3.2 Charge injection and mobility measurements

Before the measurement starts, some consideration should be made due to the use of the lateral ToF configuration. The charge created by illumination must be large enough so that the measured current can be distinguished from the thermal noise caused by the sample and external sources. To achieve a homogenous electric field across the sample:

$$\left|\vec{E}\right| = \frac{|U|}{d} \tag{5.18}$$

The charge Q injected should satisfy $Q << CU$, where U is the bias applied across the contacts and C is the capacitance (very small, typically < 1 pF). If $Q >> CU$ the charge will appreciably effect the E-field and result in a time-varying E-field. In the case of a low-field injection, the current signal I_{signal} and sample's noise current I_{noise} (from the pre-amplifier and input resistor R) can be calculated using Eq. (5.19) and Eq. (5.20) respectively, where full charge collection and constant current have been presumed.

$$I_{signal} = \frac{Q\mu U}{d^2} \tag{5.19}$$

$$I_{noise} = 4\Delta f \sqrt{k_B TC} \tag{5.20}$$

Here μ is the carrier mobility and Δf is the bandwidth of the RC circuit ($\Delta f = 1/(4RC)$). Having this information, the signal-to-noise-ratio can be used to estimate the charge Q needed in a particular experimental situation.

To calculate the carrier mobility, in this case the low-field hole mobility (μ_h), the drift velocity must first be determined as a function of the bias voltage as shown in Eq. (5.21).

To extract the low-field hole mobility we assume the semi-empirical expression:

$$\left|\vec{v}_d\right| = \frac{d}{\tau_h} = \frac{\mu_h \left|\vec{E}\right|}{1 + \frac{\mu_h \left|\vec{E}\right|}{v_{sat}}} \tag{5.21}$$

Where τ_h is the transit time (t_1-t_0) from Eq. (5.17) and v_{sat} is the saturation velocity. (5.21) can be rewritten:

$$\tau_h = \frac{d}{v_{sat}} + \frac{1}{|U|} \cdot \frac{d^2}{\mu_h} \tag{5.22}$$

The slope and intercept of a linear least squares fit of τ_h to $1/U$, e.g. as exemplified in Fig. 5.7, provides the information needed to acquire mobility and saturation velocity.

$$\mu_h = \frac{d^2}{a_h} \quad and \quad v_{h,sat} = \frac{d}{b_h} \tag{5.23}$$

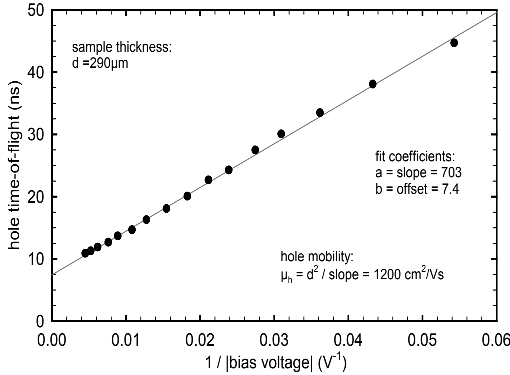

Figure 5.7 Hole ToF curve vs. inverse bias for a CVD diamond sample is shown in the plot. The hole mobility in this case is μ_h = 1200 cm^2/Vs.

5.4 Infrared detectors

IR detectors can be characterized by two figures-of-merit: signal-to-noise ratio, i.e. the electronic signal quality and Temperature Coefficient of Resistance (TCR). There are two different categories of IR detectors available on the market: photon detectors and thermal detectors. In the first group radiation absorption causes electron transition between the different bands. While fast response and high signal–to–noise performance are the main advantages of these detectors, they are dependent on cryogenic cooling to reduce the noise caused by the thermal generation of the charge carriers. Thermal detectors do not suffer from this drawback and operate at room temperature. These detectors have a slower response and poorer heat sensitivity but they are much cheaper to produce.

5.4.1 Thermal detectors (TDs)

Since the advent of thermal detectors, particular attention has been given to devices, materials and their growth techniques that can maximize the thermal responsivity. Thermal detection occurs in the "thermistor" material or structure. When a TD array is illuminated by an IR image, the temperature of individual detector elements will vary with temperature, resulting in an electronic image of the infrared scene. The resistivity is an exponential function of the ratio between the thermal activation energy and the absolute temperature, i.e.:

$$\rho = \rho_0 \exp\left(\frac{E_a}{k_B T}\right) \tag{5.24}$$

where ρ, ρ_0, E_a and k_B are the resistivity, measured pre–factor, activation energy and Boltzmann's constant. As a figure of merit, for thermal detection, the temperature coefficient of resistance has been used to quantify the temperature sensitivity [45]. The relation between TCR and the activation energy is defined as:

$$TCR(T) = \frac{1}{R}\frac{\partial R(T)}{\partial T}\left[K^{-1}\right] = -\frac{E_a(T)}{k_B T^2}\left[K^{-1}\right] \tag{5.25}$$

where R is the resistance. The TCR depends on the mobility, the carrier concentration and the compensation ratio. In semiconductors, this can be expressed by the activation energy derived from the Arrhenius plot (second part of Eq. 5.25). Thermistors are further classified as "Positive Temperature Coefficient" devices (PTC devices) such as metals and "Negative Temperature Coefficient" devices (NTC devices), including semiconductors. The operating temperature for diamond is reported to be up to 1000˚C [46]. This makes diamond a challenging competitor for high temperature sensing applications. Thus, semiconducting wide bandgap diamond, due to its high melting point, stability at high temperature, resistance to chemical attacks, small specific heat, and high thermal conductivity is a superior material to be used for high temperature sensors, high-power and high speed electronics [47-49]. The perspective is that the diamond thermistor could work fully at higher temperature and overcome the operational limits shown by other conventional thermal detectors [51, 52]. The study in **Paper VII** presents Schottky diodes made of Al/diamond with outstanding properties and performance for high temperature sensors.

5.4.2 Schottky detectors

Schottky-diodes have been used widely as thermistors and were introduced as microbolometers at Bell Labs [53]. A thermal detector senses IR radiation by temperature modulation of thermionic emission current within a Schottky diode. The reverse bias current of a Schottky diode varies exponentially with temperature but can be considered approximately linear for small temperature variations. The sensitivity to temperature variations is mainly determined by the Schottky barrier potential and is influenced less by the applied bias. Due to the potential barrier and high resistance at the MS interface, the current flow is rather low. Since *1/f* noise is proportional to the current and the current is very low, Johnson noise will dominate as the main noise source in these devices. The MS interface resistance and consequently the Johnson noise can be reduced by improving the contacts. On the other hand, noise sources such as carrier interaction with surface states and defects are always present in semiconductors.

From thermionic emission theory, [54] it is possible to calculate the current density in a Schottky diode based thermal detector. During the reverse bias operation, at large voltages compared to $k_B T/q$, the reverse current density J_R reduces to the saturation current density:

$$J_R = J_S = A^* T^2 (\exp(\frac{-q\phi_B}{k_B T})) \tag{5.27}$$

The change in the reverse current in a thermionic detector as a function of temperature, is given by:

$$\frac{\partial J_R}{\partial T} = T\left(\frac{q\phi_B}{k_B T} + 2\right) A^* (\exp(\frac{-q\phi_B}{k_B T})) \tag{5.28}$$

Finally the temperature coefficient of resistance is expressed as:

$$TCR(T) = \frac{1}{J_R}\frac{\partial J_R}{\partial T} = \frac{1}{T}\left(\frac{q\phi_B}{k_B T} + 2\right) \tag{5.29}$$

At ambient temperature, the use of thermionic emission based TDs in uncooled thermal imaging, offers advantages of improved performance, simpler fabrication and potential cost reduction. But it is at elevated temperatures that these devices show their high performance ability as thermal imaging sensors.

6 Summary of the results

Different electrical properties of single crystal CVD diamond have been studied by different measurement techniques. The results have been described in **Papers I-VII**. A brief summary of these results will follow in this chapter.

6.1 Compensation in boron-doped diamond

From Hall-measurements in **Paper I**, in the temperature range of 80-450K, and from best fits using Eq. 5.5, we observed a volume fraction lower than 10^{-4} between the compensating donor (N_D) and the dopant concentration, (N_A) in the best samples. The acceptor concentration obtained from fits to Hall data matched the data from capacitance-voltage measurements performed on Schottky diodes.

Secondary ion mass spectrometry was used as a complementary method to measure the total boron concentration in the samples. The data are summarized in Table 6.1.

Table 6.1 Summary of the results with 95% confidence interval. The Hall mobility at room temperature μ_H is also included.

Hall-effect measurements					***C-V***	***SIMS***
Sample	**E_A (eV)**	**N_A (cm^{-3})**	**Comp. ratio**	**μ_H (cm^2/Vs)**	**N_A–N_D (cm^{-3})**	**[B] (cm^{-3})**
1	0.37±0.02	$4.8\pm3.7\times10^{18}$	$< 10^{-4}$	435	$7\pm1\times10^{17}$	$1.5\pm0.3\times10^{18}$
2	0.34±0.01	$1.5\pm0.5\times10^{18}$	< 0.09	365	$2.4\pm0.3\times10^{18}$	-
3	0.36±0.01	$2.9\pm0.9\times10^{18}$	$< 10^{-4}$	285	$1.8\pm0.2\times10^{18}$	$3.9\pm0.8\times10^{18}$

Table 6.1 shows that the activation energy values for all samples lie below 0.37 eV and exhibit a dependency on the boron concentration. The total boron concentration [B] was obtained from SIMS measurements. These values were higher than the corresponding value obtained from *C-V* measurements, indicating that boron has been partially passivated. The hole concentration dependence on the temperature in Fig. 6.1 follows the semiconductor theory described in chapter 5 (c.f. Fig. 5.1).

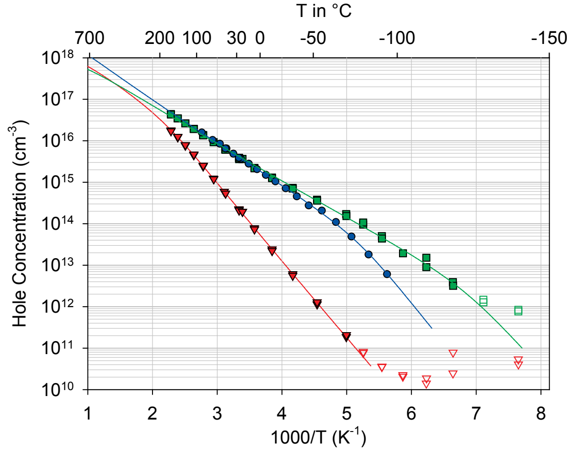

Figure 6.1 Hole concentration versus reciprocal temperature including best fits to Eq. (5.5). Filled symbols denote data for which valence band conduction is believed to be the dominant conduction mechanism.

The hole concentration behavior at low temperature is most likely caused by hopping conduction. Samples 1 and 3 show extremely low compensation ratios but in sample 2, the high concentration of donors shifts the transition from partially to completely ionized compensation towards higher temperature.

6.2 Lateral time-of-flight measurements on thin SC-CVD layers

Charge carrier dynamics in intrinsic homoepitaxial diamond film were investigated using the lateral time-of-flight measurement system described in **Paper III**. Both bulk CVD diamond samples and samples consisting of a thin layer of CVD diamond on top of a *Ib*-substrate were investigated. Electron-hole pairs were created in between two parallel metal contacts on the surface with a contact spacing of 0.3 mm, using a 213 nm UV pulsed laser. The light was focused into a line in parallel to the contacts and at a distance of 15 µm from one contact edge. Bias voltages in the range of 10-300 V were applied across the contacts. A hole transit could be observed in the current traces. Examples of such traces are shown in Fig. 6.2.

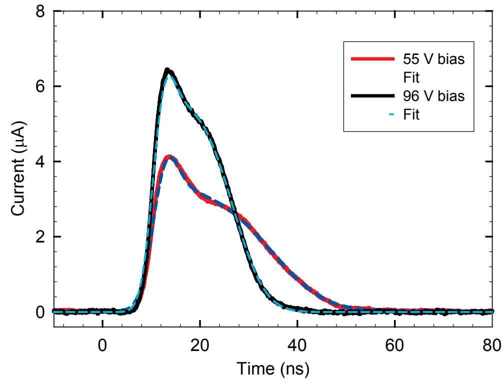

Figure 6.2 Fits of Eq. (5.17) together with experimentally measured currents (hole transport, average over 100 shots) for two different bias voltages.

In the thin layer samples, a linear relation between the drift velocity and bias voltage was revealed, by observing hole transit signals near the surface. A hole mobility of μ_h = 860 cm^2/Vs from the slope of the fit in Fig. 6.3 could be obtained in the best sample.

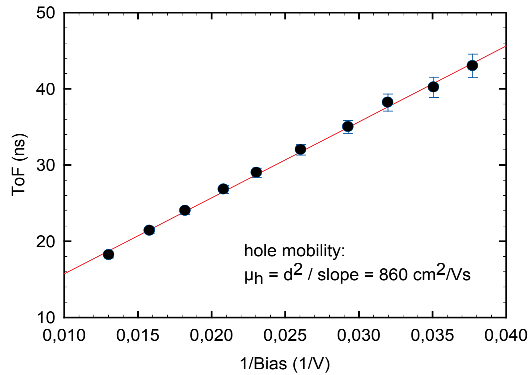

Figure 6.3 The transit time τ_{tof} from the fits in a thin layer sample has been plotted vs. reciprocal bias voltage (1/V).

From the experimental data measured on the bulk sample, a hole mobility of μ_h = 1200 cm^2/Vs could be calculated. The τ_{tof} in both cases is defined as $\tau_{tof} \equiv t_1 - t_0$ from Eq. (5.17). In contrast to the vertical ToF, the obtained mobility values are much lower. Anisotropy in the observed carrier mobility could possibly be explained by the surface scattering effects and scattering caused by dislocations aligned with the growth direction.

6.3 Characterization of single crystal CVD diamond Schottky barrier diodes

In this work (**Paper II),** freestanding single crystal CVD diamond was used to make Schottky diodes both on *p*-type material (*p*) and *p*-type material with a thin intrinsic overlayer, (*p-i*). Internal photo-emission (IPE) measurements in combination with other characterization techniques such as current-voltage and current-temperature were used to investigate the barrier height of the samples with different metallizations (Au, Ni and Al).

The diodes showed a barrier height, attributed to the interface Schottky metal and boron doped diamond, ranging from Φ_B=1.78-2.10 eV, using the internal photo-emission technique (Fig. 6.4). The results are summarized in Table 6.2.

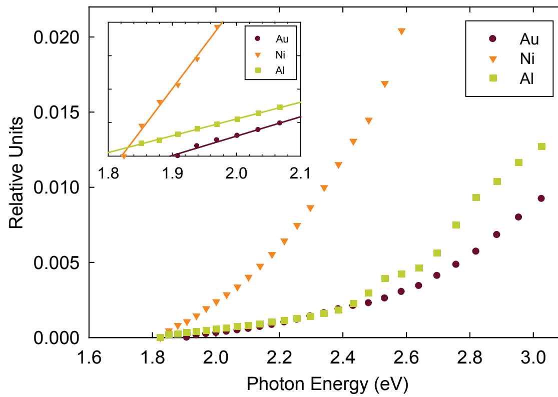

Figure 6.4 Fowler plot for sample *A* with three different metallizations. The inset is a detail of the linear regression region.

Table 6.2 Schottky barrier heights as obtained from internal photo-emission spectroscopy measurements on two samples A & B for three different Schottky metals.

Φ_B**(eV)**	**Au**	**Ni**	**Al**
A	1.91	1.82	1.78
B	2.10	2.0	1.91

Lower Schottky barrier height values were obtained using *I-V* or *I-T* methods, i. e. Φ_B=1.00-1.71 and relatively high ideality factors, above 1.4, were also observed. The presence of interfacial defect states might cause this behavior. A comparison between these methods showed that, $\Phi_B(I\text{-}T) \leq \Phi_B(I\text{-}V) < \Phi_B(\text{IPE})$. The lower sensitivity of IPE to interface damage which introduces interface states or recombination centers causing trap-assisted tunnel currents (larger $n \leftrightarrow$ lower Φ_B) is a likely a reason for this difference.

6.4 Electron and hole drift velocity measurements in CVD diamond

To achieve better understanding of the carrier transport in the SC-CVD diamond, drift velocity of both electrons and holes were investigated in a broad temperature range of 83-460 K. For this study (**Paper IV)**, three high quality samples were analyzed using a time-of-flight system. Observations show very little spread among the different samples, indicating low defect and impurity concentration in the diamond crystal. Neither did the choice of different contact metals -Ti/Al or Ni influence the measurements.

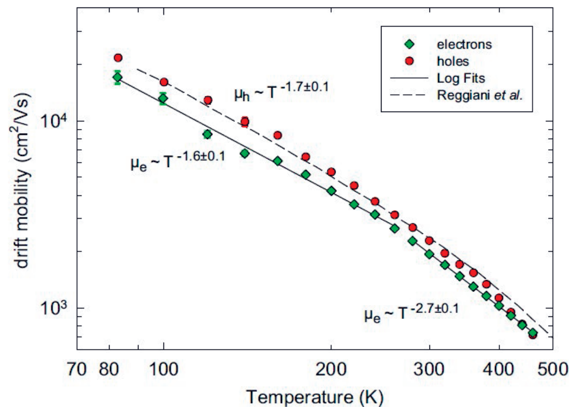

Figure 6.5 Low field drift mobilities for electrons and holes in the temperature range 83–460 K.

Fig. 6.5 shows the distinctive drift mobility behavior for both electrons and holes. At temperatures below 280 K the dominating acoustic phonon scattering leads to a typical $T^{-3/2}$ dependency, where the steeper slope for $T > 280$ K, indicates the onset of intervalley phonon scattering. This is in good agreement with previous findings and theoretical calculations [55].

Furthermore, low-temperature time-of–flight measurements were used to measure very low impurity concentrations (**Paper VI**). The measurement was carried out in the temperature range 10 - 80 K and hole transport properties of boron-doped single crystal CVD diamond, grown in the <100> crystallographic direction, were investigated. To be consistent, the same high-purity diamond samples as in (**Paper IV**) were used to study hole drift mobility in the low-injection regime and the scattering mechanisms involved in the process. A saturation of the hole mobility was observed. This indicates that impurity scattering is the dominating scattering process at these low temperatures.

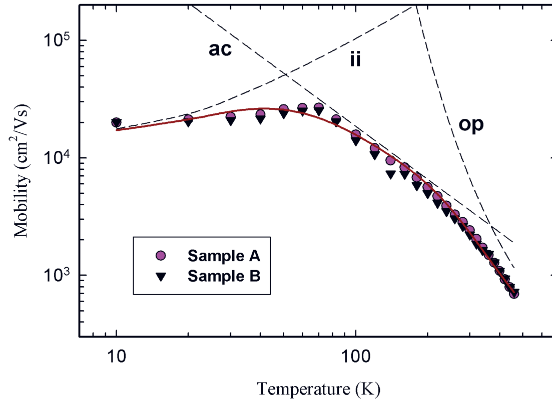

Figure 6.6 Low –field drift mobility data for samples A and B. The solid line shows the best fit according to the model described in **Paper VI**.

6.5 Negative electron mobility in diamond

Hot electron transport properties in CVD diamond have been investigated using the time-of-flight technique with the purpose of elucidating the origin of the negative differential mobility (NDM) observed at low temperatures and high electric fields (**Paper V)**. In this paper we report NDM in diamond in the <100> crystallographic directions and we explain it in terms of conduction band valley repopulation.

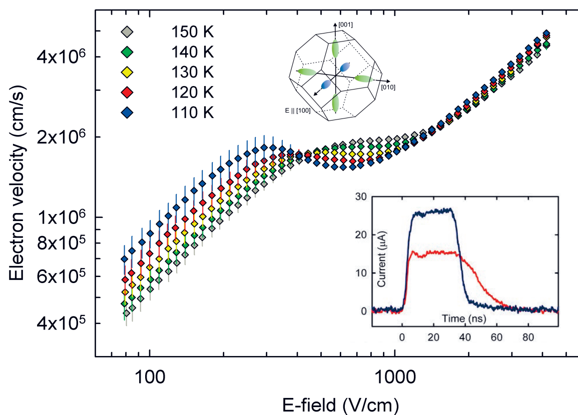

Figure 6.7 Electron drift velocity in diamond vs. electric field applied along the [100] axis for five different temperatures. Inset shows examples of measured current traces for 500 (red) &1350 (blue) V/cm at 120 K. The hot (green) and cold (blue) valleys are shown in the Brillouin zone.

This effect originates from the different response of the two longitudinal electron (cool) valleys parallel to the field and the four transversal electron (hot) valleys perpendicular to the field with their respective effective masses m_l^* and m_t^*, in the direction of the electric field. The data were obtained from measurements on three different samples. NDM could be observed in the data at temperatures below 140 K and an electric field between 300 – 600 V/cm. The results are summarized in Table 6.3.

Table 6.3 Summary of the findings from drift velocity measurements for T = 110-140 K.

Temp-erature (K)	Peak velocity ($\times 10^6$ cm/s)	E-field at peak (V/cm)	Valley velocity ($\times 10^6$ cm/s)	E-field at valley (V/cm)	Low-field mobility (cm^2/Vs)	Mini-mum NDM (cm^2/Vs)	E-field at mini-mum (V/cm)
110	1.83	290	1.54	620	7010	-1810	410
120	1.73	410	1.62	670	5980	-630	480
130	1.76	520	1.73	670	5480	-220	570
140	1.84	760	1.84	760	5040	0	760

6.6 Temperature Sensors using SC-CVD Diamond Schottky Diodes

Certain high temperature electronics applications require a material for advanced semiconductor devices, which can operate at 600˚C where conventional silicon-based electronics cannot function. Diamond's ability to function at high temperature, high power, and high radiation conditions enables large performance enhancements to a wide variety of systems and applications, e.g. electric vehicles, space exploration and nuclear reactors.

The evaluation of the thermal response of the diamond/metal junction was carried out by fabrication of Schottky diodes on SC-CVD diamond samples for different doping levels (**Paper VII**). The TCR was analyzed in 25 ˚C temperatures steps in the range of 25 – 300 ˚C. The noise characterization was performed at a fixed bias voltage of 1 V, which is an appropriate working voltage for the thermal detectors. An increase in forward bias did not effect the thermal responsivity, although TCR values slightly declined by the temperature rise. Fabricated detectors demonstrate excellent TCR values (TCR > |-10 %/K|) at working temperatures up to 473K and noise level in the range of 1.8×10^{-14} (V^2/Hz) at RT. Table 6.4 summarizes the estimated parameters of our Schottky diodes in this study.

Table 6.4 Summary of estimated activation energies, barrier potentials at Aluminum/Diamond interface, TCRs, noise constants and R at 1V bias voltage for the detectors.

	A	***B***	***C***	***D***
Activation energy [eV], 150 ˚C	0.75	1.05	1.2	2.22
MS potential barrier [eV]	0.69	1.06	1.25	2.4
-TCR [%/K], 150 ˚C	4.95	7.32	8.56	16.04
-TCR [%/K], 200 ˚C	4.27	4.77	5.28	10.72
Noise constant [$K_{1/f}$]	6.7×10^{-15}	6.6×10^{-15}	6.6×10^{-15}	1.8×10^{-14}
Resistance, 150 ˚C [Ω]	120×10^{3}	689×10^{9}	122×10^{9}	9.9×10^{9}

7 Conclusion

The aim of this work has been to study some of the electrical properties of single-crystal CVD diamond. Although the quality of diamond thin films has improved during the last decade, the way to achieve successful diamond based devices is still surrounded by many uncertainties.

The concentration of impurities and dopants and thereby the compensation ratios have in diamond thin films has been studied, using different characterization techniques. From Hall-effect measurements, a very low compensation volume fraction in *p*-type CVD diamond was reported. This was in good agreement with data obtained from SIMS and *C-V* measurements. An important consequence of the study is the realization of devices with reasonable carrier density and increased hole mobility.

A Schottky barrier height study of different contact metals was performed on CVD diamond films because of the importance of understanding the forward voltage drop and voltage blocking. The behavior of the Schottky contacts exhibits strong Fermi level pinning related to a high concentration of interface states.

To study the effect of surface properties on carrier transport close to a surface, a time-of-flight system with lateral configuration has been described and hole transport measurements on homoepitaxial diamond thin film have been performed. It is obvious that the result is highly affected by surface scattering effects and scatter from dislocations, aligned in the growth direction. A better surface treatment method must be introduced. Furthermore, the improvement of the growth control is essential to reduce dislocations and other defects.

Low-temperature time-of-flight measurements were used to measure very low impurity concentrations and to investigate carrier drift velocity in SC-CVD diamond. This work explains the limitation of the drift velocity by identifying which scattering mechanisms dominate within certain temperature intervals. The hole drift velocities proved to be in good agreement with the data for ultra-pure natural diamond in previous studies. In addition, field-dependent conduction valley repopulation has been observed for the first time for electrons at low temperatures, leading to negative electron mobility. In addition, the results show significant improvement in the quality of the synthetic diamond indicated by the extremely small spread across the different samples studied.

Single crystal synthetic diamond proved to be an excellent candidate for use as a thermal detector and IR imaging applications. Measurements on diamond based Schottky diodes demonstrate that due to a high potential barrier at the metal/semiconductor interface, very high TCR can be obtained at elevated temperatures. Fabricated detectors exhibit a very low noise level indicating the high crystal purity of these samples. Nevertheless, the growth technique of diamond and the stability of metal contacts play a very important role in the performance of the detectors.

8 Summary of papers

A short summary of the **Papers I -VII** followed by the author's own contribution is specified in this chapter.

Paper I

Compensation in boron-doped CVD diamond

The paper deals with the important fact that deep level defects and residual impurities cause compensation effects, leading to a reduced free carrier concentration. Very low compensation ratios below 10^{-4} were recorded from Hall-effect measurements and were found to be in agreement with data obtained from both *C-V* and SIMS measurements.

The author made minor contributions, since he just started his PhD, by participating in sample preparation and the literature survey.

The paper is published in Physica Status Solidi (a) ***205*** *(9), 2190-2194 (2008).*

Paper II

Characterization by internal photoemission spectroscopy of single crystal CVD diamond Schottky barrier diodes

Fundamental electrical properties of Schottky barrier diamond diodes were studied using photoemission spectroscopy in combination with complementary *I-V* and *I-T* methods. Depending on the boron concentration and the choice of Schottky metal, the highest Schottky barrier heights were obtained from the least surface defect sensitive method – photoemission spectroscopy. Relatively high ideality factors were also observed. This can be attributed to large spatial variations of the Schottky barrier height.

The author has been deeply involved by preparing the samples, performing the measurements and analyzing the data. He has also done most of the writing and the literature survey.

The paper is published in Journal of Electronic Materials, ***39****, 8, 1203-1208 (2010).*

Paper III

A lateral time-of-flight system for charge transport studies

Understanding the influence of different surface conditions and surface properties on transport dynamics in thin films is essential in many potential

device applications. For this reason, we have built a lateral ToF system for studying charge carrier transport in intrinsic diamond. A hole drift mobility of about 860 cm^2/Vs was observed in thin films.

The author has contributed in building the setup, performing the measurements, taking part in evaluation of the data and he did the literature survey.

*The paper is published in Diamond & Related Materials **18**, 1163–1166 (2009).*

Paper IV

Electron and hole drift velocity in CVD diamond

In this paper we have investigated low-field drift mobilities for electrons and holes in the temperature interval 83 - 460 K and for electric fields between 90 and 4000 V/cm. In order to minimize the effect of space charge on the applied electric field, measurements were performed in the low-injection regime. For temperatures below 280 K acoustic phonon scattering was pointed out as the dominating scattering mechanism, whereas for T > 280 the carrier drift velocity was limited by optical phonon scattering.

The author was involved in preparation of the samples, performing the measurement, contributed to the evaluation of the data and wrote a minor part of the paper.

*The paper is published in Journal of Applied Physics **109**, 063719 (2011).*

Paper V

Negative electron mobility in diamond

The conduction valley distribution of electrons drifting in an external electric field was investigated. We observed negative differential mobility (NDM) in the [100] direction in diamond below 140 K, at fields in the range 300-600 V/cm. This can be explained by repopulation effects between different conduction band valleys through hot-electron carrier scattering.

The author participated in doing the literature survey, preparing the samples and he was involved in performing the measurements.

*The paper is published in Applied Physics Letters, **100**, 172103 (2012).*

Paper VI

Low temperature hole transport in single crystal synthetic diamond

Low-temperature time-of-flight measurements were used to measure very low impurity concentrations. The measurement was carried out in the temperature range $10 \leq T \leq 80$ K on boron-doped single crystal CVD diamond, grown in the <100> direction. The hole drift mobility in the low-injection regime, and the scattering mechanisms involved in the process, were investigated. Saturation of the hole mobility was observed for the first time, indi-

cating that impurity scattering is the dominating scattering process at these low temperatures.

The author has made a major contribution by preparing the samples, performing most of the measurements, evaluating the data and writing the paper.

The paper is submitted to Physical Review B (2012).

Paper VII

High performance temperature sensors using SC-CVD diamond Schottky diodes

Outstanding electrical and thermal properties of diamond make it a suitable candidate as a thermistor material. Diamond Schottky diodes were studied for IR detection and imaging at high temperatures. The study shows that single crystal CVD diamond form a high potential barrier at the metal/semiconductor interface, which results in a very high thermal coefficient of resistance (TCR). Although a high TCR value and a low noise level were obtained, the performance of these detectors can be improved by optimizing the contact stability and growth technique.

The author has been the main responsible for planning the study, preparation of the samples, performing the measurement, evaluation of the data and writing the paper.

The paper is submitted to Applied Physics Letters (2012).

9 Suggestions for future work

This work includes a study of some electrical properties of SC-CVD diamond. We have applied a variety of experimental techniques such as ToF, Hall, *C-V* and photocurrent to analyze diamond samples. In Uppsala, there are many groups, working with diamond, who are specialized in different techniques. Further collaboration between these groups would benefit the development of diamond-based devices and could address some unsolved problems. There are some projects, which have already been started, on which I will focus further.

9.1 Defect investigation of SC-CVD diamond

To understand the electrical behavior of CVD diamond, it is very important to investigate the defects inside the crystal lattice. Generally, only defects which introduce levels in the band gap affect the electrical and optical properties of a material. They can be stable or unstable (charge state of the defect changes) and are of great importance to investigate. Single-crystal CVD diamonds can be pure and almost free from crystal defects such as dislocations and grain boundaries. However, there are several defects present in the non-equilibrium charge states with long lifetime, acting as deep traps for carriers [56, 57].

The conventional experimental techniques, which have been used to analyze defect levels, such as Thermally Simulated Current (TSC) and especially Deep Level Transient Spectroscopy (DLTS), are rather difficult to perform on diamond. The requirement of having low defect concentration, as discussed in **Paper I,** might be one of the aspects. Another reason is the wide bandgap of diamond (5.47 eV), which requires extremely high temperature (~1000°C) to excite all trap centers.

To achieve high temperature, we are attempting to develop a high temperature DLTS-setup where the measurements will take place in a vacuum chamber in the temperature range 700-1000°C. Fig 9.1 and 9.2 on the next page describe the schematics of the DLTS setup, which is fully operational but needs some final calibration.

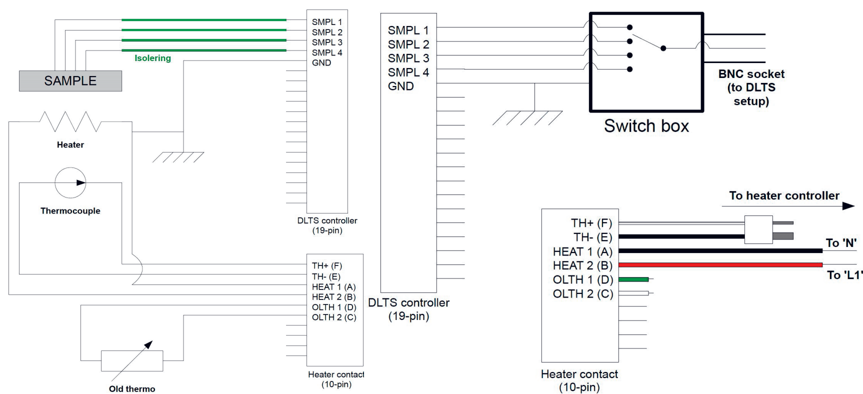

Figure 9.1 Electrical network schematics of DLTS apparatus.

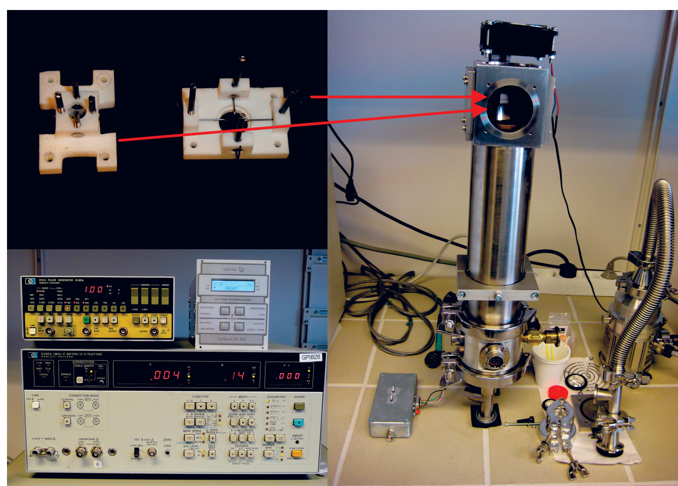

Figure 9.2 Schematic sketch of a high temperature DLTS apparatus. (on the top left) Insulating sample holder, (on the bottom left) the HP 4280A C-V plotter, used as a fast capacitance meter and pulse generator in our DLTS experiment. (to the right) The cryostat connected to a turbo pump and a diode switching box.

9.2 δ-doped diamond

One of the main limitations of using active electronic diamond devices is associated with the deep boron acceptor and the lack of any reliable n-doping technology with shallow donors. Full activation of boron can only be

obtained at high concentrations, above 10^{20} cm^{-3}. On the other hand, the maximum sheet charge density in a FET channel, which can be modulated prior to the electrical breakdown of diamond, is about 4×10^{13} cm^{-2} [58]. This limitation leads to the concept of delta doping. The growth of very narrow type *p*-doping spikes in diamond has allowed obtaining δ-doped systems that can be used in the fabrication of high drain current field effect transistors [59]. Conduction takes place when free carrier diffusion into the intrinsic layer results in high carrier mobility due to reduced scattering at the ionized acceptors (Fig. 9.3). Hall-effect measurements on δ-doped diamond allow us to gain new understanding of carrier transport in delta-doped structures.

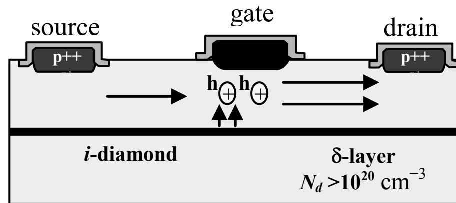

Figure 9.3 Highly boron-doped delta-layer SC-CVD diamond used to create a channel with high mobility.

However, a simple bulk conduction description cannot be applied to this configuration. The situation is more complicated for a delta doped device. Here conduction occurs both in sub-bands confined to the delta doped layer as well as in the valence band. An increase of thermal energy will excite holes from the sub-bands with lower mobility, into the valence band, with a higher mobility. Therefore a quite sophisticated physical model which takes this into account is required.

9.3 High voltage (HV) breakdown diodes

There is great interest in the Division for Electricity in developing diamond-based diodes with low on-state resistance of the drift layer and high breakdown voltage to be used as rectifiers. The Division is working with renewable energies such as wave and wind power where a test farm of wave power generators has already been planned and prototypes are currently tested in Lysekil. One of the main electrical challenges is to be able to feed the current directly into electrical grid (50 Hz) due to the variation in both frequency and amplitude of the generators [60]. That is why it is desirable to design Schottky diodes which could perform e.g., at 1.7kV-50A. The diode should provide a path for the reverse current flow whenever inductive loads are

switched off and must have good reverse recovery characteristics. Intrinsic single crystalline CVD diamond diodes could satisfy these demands.

To achieve such a diode, a termination technique must be developed to prevent a premature breakdown at the surface of the device. The proper termination design distributes the electric field evenly by enlarging the space charge region at the edge of the junction. Having overcome these problems one can produce electrically and economically efficient converters.

Acknowledgements

First of all I would like to express my sincere gratitude to my supervisor, Professor Jan Isberg for his guidance and encouragement and for involving me in this interesting field. Secondly, I would like to thank my assistant supervisor, Professor Mats Leijon, head of the Electricity Division for injecting positive energy into the Division and making me feel welcome.

I am also grateful to my former supervisor Professor Anders Hallén for all encouraging discussions and explanations; I value it more than you know. Dr. Henry Radamson must be acknowledged for his guidance and all the valuable things he taught me.

I extend my appreciation to my office-mates, Markus Gabrysch, Kiran Kumar Kovi and Florian Burmeister, for their friendship and counsel and helping me to understand many aspects of my work.

A special thank you to my dear friends and colleagues at the division, specially Juan de Santiago, Janaina Goncalves de Oliveira, Johan Abrahamsson, Valeria Castellucci and Hamid Sarve for making my life richer.

I would like to acknowledge in particular Gunnel Ivarsson, Thomas Götschl, Ingrid Ringård and Ulf Ring who have helped me with their competence and interesting dialogues. Many thanks to the Microstructure Laboratory staff, specially Rimantas Bručas and Farhad Zamany for all their help with cleanroom processing.

I would also like to thank Element Six, Ericsson Research Foundation, Vetenskapsrådet, Stiftelsen för Miljöstrategisk Forskning (MISTRA) and Ångpanneföreningens Forskningsstiftelse for supporting financially our projects.

Finally, I would like to express my gratitude to you Erika, my sons Elias and Samuel and my dear family for all their understanding and endless love. I would not be here without your support.

Svensk Sammanfattning

Diamant besitter extrema egenskaper som gör materialet väldigt attraktivt för användning inom olika områden. Diamant har hårdhet 10 på Mohs skala, det är det hårdaste material som finns i naturen och används flitigt inom industrin för skärande bearbetning samt slipning av andra material. Egenskaper såsom hög kompatibilitet med mänsklig vävnad tillsammans med en utmärkt stabilitet i kemiskt aggressiva miljöer gör diamant åtråvärd i medicinska applikationer. Det äldsta och troligen mest kända användningsområdet är att utnyttja diamants enastående ljusbrytning för att tillverka smycken. Det är dock diamants elektriska egenskaper gör materialet intressant för högteknologiska användningar.

Ren, icke förorenad, diamant är en isolator. Under rätt förutsättningar har diamant dock utmärkta halvledaregenskaper passande för elektroniktillämpningar. Materialet har ett brett bandgap (5.47 eV) som tillsammans med dess höga värmeledningsförmåga gör det tilltalande i åtskilliga applikationer. Exempel på detta är kraftelektronik och högfrekvenstillämpningar. Man har kunnat tillverka syntetisk diamant i högtrycks- och högtemperaturprocesser under flera decennier. Trots detta är det först nu på senare år som intresset för diamant inom elektronik har tilltagit. En nackdel har varit avsaknad av tillräckligt defektfritt och rent material som kan uppfylla kraven för tillverkning av elektroniska komponenter. Nya metoder möjliggör framställning av enkristallin syntetisk diamant genom en kemisk ångdeponeringsprocess där man använder en blandning av vätgas och metan (Chemical Vapor Deposition, CVD). I dag är det möjligt att tillverka enkristallina diamantfilmer, ca 10x10 millimeter stora, med hög renhet.

Med tillgång till sådana prover kan nu forskare över hela världen omvandla teoretiskt erhållna resultat till experimentella analyser och djupare undersöka diamants elektriska egenskaper. En teknik som kan tillämpas för att analysera kristallkvalitet eller närmare bestämt diamantkristallens förmåga att transportera laddning är den s.k. Time-of-Flight (ToF) metoden. Tekniken kan användas för indirekt undersöka existens av defekter och laddningsfällor och begränsande mekanismer som påverkar laddningsbärare i tunna lager. Experimentet utförs genom att man formar metallelektroder på diamantytan och belyser ena elektroden med t. ex en UV laser med tillräcklig hög fotonenergi för att skapa elektron-hål par i provet. Strömmen genom provet mäts som funktion av tiden och man kan då beräkna den tid det tar för laddningsbärare att förflytta sig mellan elektroderna. Genom att applicera en

spänning med önskad polaritet mellan kontakterna, är det möjligt att analysera hål respektive elektroner separat. Information om rymdladdning i provet m.m. fås genom att studera den tidsvarierande strömmen. Dess studier bidrar till att utöka vår kunskap om diamants elektriska egenskaper och resultaten är av stor betydelse för att kunna förbättra tillväxtprocessen av syntetisk enkristallin diamant.

Från de experimentella studier som presenteras i denna avhandling kan följande slutsatser dras:

- Elektriska mätningar såsom ToF, Hall-effekt mätningar, *I-V* och *C-V* på millimetertjocka diamantprover har påvisat en tydlig förbättring av kristallkvaliteten samt en minskning av föroreningar i tillgängligt material.

- Låg kompensation (<0.1%) har konstaterats genom bland annat Hall-effektmätningar i bordopade prover av enkristallin diamant. En låg kompensation är nödvändig för att erhålla hög laddningsbärartäthet i dopade komponenter.

- Lateral time-of-flight mätningar har visat sig vara ett kraftfullt verktyg vid undersökning av defekter vid eller i närheten av diamantytan. Experimentella observationer överensstämmer väl med modellering och analytiska resultat.

- Lågtemperaturmätningar ($T < 140$ K) av elektroners drifthastighet har påvisat negativ differentiell mobilitet (NDM) i diamant. Denna effekt var tidigare okänd i diamant, men är välkänd för III-V halvledare.

- Håltransportmätningar i svaga elektriska fält har utförts för temperaturer i intervallet 10 – 450 K. Temperaturberoendet hos hålmobiliteten uppvisar diverse karakteristiska beteenden i olika temperaturintervall. Detta förklaras med olika dominerande spridningsmekanismer i dessa temperaturintervall. Vid temperaturer under 80K har vi sett en mättnad av driftmobiliteten vilket indikerar att mobiliteten då begränsas av spridning mot neutrala och joniserade föroreningar i materialet.

- Vi har undersökt huruvida Schottky dioder gjorda av diamant kan användas som infraröddetektorer. En mycket hög temperaturkoefficient har påvisats, för temperaturer upp till 475 K. Detta är mycket lovande för framtida applikationer.

Bibliography

[1] J. Achard et. al. *J.Phys. D: Appl. Phys.* **40**, (2007) 6175-6188

[2] A. Hartl et. al. *Nat. Mater*. **3**, (2004) 736-742

[3] A. Lavoisier, Traité élémentaire de chimie, Paris Chez Cuchet 1789, reprinted Bruxelles: Culture et civilizations, 1965.

[4] G. Davis, ch. 1 in “CVD Diamond for Electronic Devices and Sensors” Edited by R S. Sussmann, Wiley, (2009)

[5] F. P. Bundy et. al. *J. Chem. Phys.,* **35**, (1961) 383-391

[6] H. Liander, E. Lundblad, *Ark Kemi*, **16**, (1960) 13-49

[7] W. G. Eversole, US Patent No **3**, (1962) 030,187;3,030,188

[8] E. Kohn et. al. *J. Phys. D: Appl. Phys*. **34,** (2001) R77

[9] E. Kohn et. al. *“Diamond MEMS – a new emerging technology”* Diam. Rel. Mater., **8**, (1999) 934-940

[10] W. Ebert et. al. *“High-voltage schottky diode on epitaxial diamond layer”* Diam. Rel. Mater., **6**, (1997) 329

[11] F. Celli, J. Butler, *Annu. Rev. Phys. Chem.*, **42**, (1991) 643-684

[12] C. E. Nebel, J. Ristein ”*Thin-Film Diamonds I*” Semiconductors and Semimetals, Volume 76

[13] J. P. Goss et. al. *J. Phys. Cond. Mat*., **15**, (2003) R551-R580

[14] J. Chevallier et al. "*Hydrogen-boron interactions in p-type diamond*" Phys. Rev. B, **58,** (1998) 7966

[15] K. Iakoubovskii and G.J. Adriaenssens "*Luminescence excitation spectra in diamond*" Phys. Rev. B, **61** (2000) 10174

[16] L. G. Wang and A. Zunger, *Phys. Rev.B*, **66**, (2002) 161202

[17] S. J. Sque, R. Jones, J. P. Goss and P. R. Briddon, *Phys. Rev. Lett*., **92**, (2004) 017402

[18] N. Fujimori T. Imai and A. Doi, *“Characterization of Conducting Diamond Films”* **36** (1), (1986) 99-102

[19] A. T. Collins, *“Properties and growth of Diamond”* EMIS Data review Series no 9(G. Davies Ed.), (1994) pp. 261-288, INSPEC. The Institute of Electrical Engineering, London, UK, Chapter 9

[20] T. Tshepe, C. Kasl, J. F. Prins and M. J. R. Hoch, *Phys. Rev. B*. **70**, (2004) 245107

[21] Y. Takano et. al. *Diam. Relat. Mater.*, **16**, (2007) 911-914

[22] X. Blase, C. Adessi and D. Connetable, *Phys. Rev. Lett*., **93**, (2004) 237004

[23] R. G. Ferrer, *Solid State Comm*., 7, (1969) 685-688

[24] S. Koizumi, M. Kamo, Y. Sato, H. Ozaki and T. Inuzuka, *Appl. Phys. Lett.*, **71**, (1997) 1065-1067

[25] S. Koizumi and M. Suzuki, *Phys. Stat. Sol. (a),* **203**, (2006) 3358

[26] H. Kato, et al. *Apply. Phys. Exp*., **2**, (2009) 055502

[27] H. Kato, et al. *Apply. Phys. Letter*., **86**, (2005) 222111

[28] J. Isberg et. al. *Science,* **297**, (2002) 1670-1672

[29] A. A. Quaranta, C. Canali, G. Ottvilant, *Rev. Sci. Instrum.,* **41**, (1979) 1205

[30] L. S. Pan, S. Han, D. R. Kanja, K. K. Gan and S. Zhao, et al., *Mater. Res. Soc. Symp. Proc.,* **302**, (1993) 73

[31] H. Pernegger, et. al. *J. Appl. Phys.,* **97**, (2005) 073704

[32] F. Fujita et. al. *Diam. Relat. Mater.,* 14/11–12, (2005) 1992-1994

[33] M. Nesladek, A. Bogdan, W. Deferme, N. Tranchant, P. Bergonzo, *Diam. Relat. Mater*., 17/7–10, (2008) 1235

[34] T. Collins, Breakdown field and saturation carrier velocity in diamond in *"Properties and Growth of Diamond"* Emis Data Reviews No, 9 (G. Davies Ed) pp. 288-289 (INSPEC Publications 1994a)

[35] K. Ferry, "High field transport in wide-band-gap semiconductors", *Phys. Rev. B* **12**, (1975) 2361-2369

[36] M. E. Levinshtein, S. L. Rumyantsev and M. S. Shur (Editors), *"Handbook series on semiconductor parameters"* vol. 1 (World Scientific, Singapore, 1996)

[37] T. H. Borst and O. Weis, *Phys. Status Solidi* A, **154**, (1996) 423-444

[38] J. Isberg, ch. 2 in "CVD Diamond for Electronic Devices and Sensors" Edited by R S. Sussmann, Wiley, (2009)

[39] F. Fontaine et. al. *J. Appl. Phys.,* **85**, (1999) 1409

[40] M. Willatzen et. al. *Physical Review B* **50**, (1994) 18054

[41] M. Kubovic, H. El-Hajj, J.E. Butler, and E. Kohn, *Diamond & Related Materials* **16**, (2007) 1033-1037

[42] R. H. Fowler *Physical Review,* **38**, (1931) 45

[43] D. K. Schroder, "Semiconductor Material and Device Characterization", Wiley, 2nd edition, (1998) 168-175

[44] M. Gabrysch, ch. 4 in "Charge Transport in Single-crystalline CVD Diamond" (2010) Acta Universitatis Upsaliensis

[45] L. Di Benedetto, M. Kolahdouz, B. G. Malm, M. Östling, & H. H. Radamson, *Proceedings of the 39th European Solid-State Device Research Conference* (2009) 101-104

[46] M. Aslam et. al. *Proceedings of SPIE* 1694, (1992) 184 [47] M. W. Geis et. al. *IEEE Electron Device Letters,* **8**, (1987) 341-343

[48] J. Field et. al. *The Properties of Diamond*. (Academic Press: New York, USA, 1979)

[49] K. Kobashi et. al. *Diamond film thermistor*. US Patent 5066938 (1991).

[50] J. Bonhaus, D. Borchert, A. Denisenko, & W.R. Fahrner, *Fourteenth IEEE SEMI-THERM Symposium* (1998) 139-146

[51] M. Kolahdouz, A. Afshar Farniya, L. Di Benedetto & H. Radamson, *Applied Physics Letters,* **96**, (2010) 213516

[52] G.S. Yang, D.M. Aslam, M. White, & J. McGrath, *Diamond and Related Materials* 6, (1997) 394-7

[53] J. M. Andrews & M.P. Lepselter, Solid State Temperature Sensor Employing a Pair of Dissimilar Schottky Barrier Diodes (1973)

[54] S. M. Sze, *Physics of Semiconductor Devices*, John Wiley & Sons, (1981)

[55] L. Reggiani, S. Bosi, C. Canali, F. Nava, and S. F. Kozlov, *Phys. Rev. B,* **23**, (1981) 3050

[56] M. H. Nazare and A. J. Neves, *"Properties, Growth and Application of Diamond"* 2001, London: INSPEC, Institute of Electrical Engineers

[57] L. Allers and A. Mainwood, *Diam. Relat. Mater.,* 7, (1998) 261-265

[58] A. Denisenko, E. Kohn, *Diamond & Related Materials*, **14**, (2005) 491–498

[59] A. Aleksov, A. Vescan, M. Kunze et al. *Diamond Related Materials,* **8** (1999), p. 941

[60] M. Leijon, O. Danielsson, M. Eriksson, K. Thorburn, H. Bernhoff, J. Isberg, J. Sundberg, I. Ivanova, E. Sjostedt, O, Agren, K. Karlsson and A Wolfbrandt, *"An electrical approach to wave energy conversion"*, Renewable Energy, **31** (9), (2006) 1309-1319

Acta Universitatis Upsaliensis

Digital Comprehensive Summaries of Uppsala Dissertations from the Faculty of Science and Technology 944

Editor: The Dean of the Faculty of Science and Technology

A doctoral dissertation from the Faculty of Science and Technology, Uppsala University, is usually a summary of a number of papers. A few copies of the complete dissertation are kept at major Swedish research libraries, while the summary alone is distributed internationally through the series Digital Comprehensive Summaries of Uppsala Dissertations from the Faculty of Science and Technology.

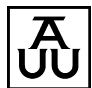

ACTA
UNIVERSITATIS
UPSALIENSIS
UPPSALA
2012

Distribution: publications.uu.se
urn:nbn:se:uu:diva-173599